Dynamics and stability of weakly viscoelastic film flowing down a uniformly heated slippery incline

Souradip Chattopadhyay [1,*] and Akshay S. Desai [2,†]
[1]Department of Mathematics, Indian Institute of Technology Dharwad, Karnataka 580011, India
[2]Department of Mechanical, Materials and Aerospace Engineering, Indian Institute of Technology Dharwad, Karnataka 580011, India

(Received 1 December 2021; accepted 9 June 2022; published 30 June 2022)

In this study, we investigate the stability of a thin viscoelastic fluid draining down a uniformly heated slippery inclined plane. A theoretical model is employed consisting of the Navier-Stokes equations coupled with the conservation equation for energy. We apply a Navier slip condition at the solid-liquid interface. To obtain the critical conditions for the onset of instability, we carry out a long-wave linear stability analysis within the Orr-Sommerfeld framework. Furthermore, we derive a first-order Benney-type evolution equation for the local film thickness to analyze the effect of long-wave instabilities. The results reveal that the slippery substrate destabilizes the liquid film flow. We find that the presence of the viscoelastic parameter and Marangoni number always promotes this destabilizing effect. We use the method of multiple scales to investigate the weakly nonlinear stability analysis of the flow which shows that there is a range of wave numbers with a supercritical bifurcation and a range of larger wave numbers with a subcritical bifurcation. The study interprets that the variation of Marangoni number, slip length and viscoelastic parameter have substantial effects on different stable or unstable zones. Different instability zones are also demarcated. Finally, the direct numerical simulations of the full thin-film model clearly demonstrate the role of the viscoelastic parameter, thermocapillary, and slip length. A good agreement between the linear stability analysis and the numerical simulations is found.

DOI: 10.1103/PhysRevFluids.7.064007

I. INTRODUCTION

In the literature, most studies on stability and dynamics of a thin-film flow down an incline are based on a Newtonian fluid model. Thin-film flow along an inclined plane with bottom heating has also been reported in several studies [1–4]. Pearson [5] and Sternling and Scriven [6] investigated thin-film flow over a heated inclined surface where they identified two thermocapillary instability modes: a long-wave mode and a short-wave mode. For a thin film flowing along a uniformly heated planar surface, Goussis and Kelley [7] studied the onset of instability in presence of the competition between the long-wave hydrodynamic and thermocapillary instabilities. To figure out the physical mechanism of primary instability, they carried out a detailed energy budget analysis for a falling liquid film over a uniformly heated substrate. They found two mechanisms associated with the thermocapillary forces and referred as an S mode (a long-wave instability) and P mode (a short-wave instability), whereas for isothermal cases, they recognized one hydrodynamic mode which is called the H mode in low to moderate values of Reynolds number. The H mode and S

*Corresponding author: sdipmath@gmail.com
†203121003@iitdh.ac.in

mode emerge in the long-wave regime while the P mode emerges in the shortwave regime. They concluded that the Marangoni number has a destabilizing nature on the long-wave H mode and S mode, as well as the short-wave P mode. Kalliadasis *et al.* [8] first demonstrated the dynamics of a thin film down a uniformly heated wall far from criticality. Several researchers, like Bankoff [9], Joo *et al.* [10], Lopez *et al.* [11], Trevelyan *et al.* [12], Ruyer-Quil *et al.* [13], Scheid *et al.* [14], and Trevelyan *et al.* [15], studied the stability of a viscous film flowing down a uniformly heated plane. The key finding from these investigations is that thermocapillarity, in general, destabilizes the flow.

However, in many technological applications, the liquids involved deviate from Newtonian behavior. The viscoelastic fluid is a subclass of non-Newtonian flows which exhibits features that are typical of both ideal fluids (viscosity) and solids (elasticity). There are various constitutive models which speak about the elasticoviscous aspect of viscoelastic fluid such as the Maxwell model, Jeffreys model, Giesekus model, Phan-Thien-Tanner model, Oldroyd model, etc. To get an overall knowledge about the different rheological models of non-Newtonian as well as viscoelastic liquids, we refer to the work of Bird *et al.* [16]. Among these models, in practical fluid mechanics, the most frequently used model is Walter's B″ model [17]. This is because the constitutive equation of this model involves only one non-Newtonian parameter. Hence one can easily obtain a deeper insight into the flow behavior of the viscoelastic fluids. Walter's B″ model is an example of a second-order model which works well where viscoelastic effects are weak. The instability of waves on a viscoelastic film was studied by Dandapat and Gupta [18]. They observed that, in the presence of surface tension, the falling film is supercritically stable and an initially growing monochromatic wave reaches an equilibrium state of finite amplitude. Later, Shaqfeh *et al.* [19] investigated the spatial instability of the Oldroyd-B fluid model. They showed that, for a small Reynolds number, although viscoelastic effects are destabilizing, the growth rate of the resulting purely elastic waves remained very small. They further concluded that, at moderate Reynolds numbers, viscoelastic effects were primarily stabilizing. Cheng *et al.* [20] performed the stability of a thin viscoelastic film of Walter's liquid B″ type down a vertical wall, using a long-wave perturbation technique. They derived a first-order surface equation in terms of the film thickness and performed both the linear as well as nonlinear stability analyses. Based on the momentum integral approach, Andersson and Dahi [21] investigated the flow of a viscoelastic liquid film along a vertical wall. They showed that the viscoelastic film develops more rapidly than a Newtonian liquid film towards the downstream asymptotic state. Uma and Usha [22] demonstrated two-dimensional long and stationary waves of finite-amplitude on a thin viscoelastic fluid flowing down an inclined plane, where they discussed different bifurcation scenarios. Dandapat and Samanta [23] extended the work of Cheng *et al.* [20]. They derived both the first- and second-order Benney-type surface equations. They observed the destabilizing effect of the viscoelastic parameter. Using the weighted residual integral method, Amatousse *et al.* [24] investigated the flow of a thin layer of Walter's B″ viscoelastic fluid flowing down an inclined plane. They showed the destabilizing nature of the viscoelastic parameter on the flow field. In addition, they discussed the influence of viscoelastic parameters on the nonlinear development of the traveling waves. Fu *et al.* [25] studied the stability of Walter's B″ viscoelastic film flowing down an incline in the presence of thermocapillarity. They showed that both heating and viscoelasticity destabilize the flow. Sharma *et al.* [26] showed that the influence of the elasticity on the stability of the inertialess flow is significantly affected by the geometrical characteristics of the substrate. They concluded that the topography initially exerts a destabilizing influence as the wavelength of the periodic wall increases whereas the topography may stabilize the flow for shorter wall wavelengths. In literature, not many experimental works on the non-Newtonian fluids were reported. As far as our knowledge is concerned, for the flow of a thin viscoelastic liquid along a heated plane in the presence or absence of the slip, no experimental work has been performed. However, Allouche *et al.* [27] conducted an experiment to investigate the primary instability of a shear-thinning film flowing down an incline. The shear-thinning fluid is a time-dependent non-Newtonian fluid that does not belong to the same class as the viscoelastic liquid. However, this provides some ideas about the flow instability and the behavior of the non-Newtonian

fluid in a real situation. In their experiment, they used a mixture of carboxymethylcellulose (CMC, E466) and xanthan gum (E415) as shear-thinning fluids that obeyed the Carreau law. This was the first experimental study where they demonstrated evidence of the destabilizing effect of the shear-thinning behavior in comparison with the Newtonian case.

The above-mentioned studies employed the classical no-slip boundary condition at the solid-liquid interface. Within the framework of the Orr-Sommerfeld analysis, Pascal [28] studied the stability characteristics of a Newtonian thin-film flow and showed the effect of the porous substrate on the primary instability. In this study, he considered a thin liquid film flow over an inclined porous substrate with the Navier-slip boundary condition $u = L_s \partial_z u$, where u is the tangential velocity, L_s is the effective slip length, and $\partial_z u$ is the velocity gradient. The Navier-slip boundary condition states that the velocity at the boundary is proportional to the tangential component of the wall stress, which is similar to the boundary condition used by Beavers and Joseph [29]. Samanta *et al.* [30] first discussed the primary instability for a thin film down a slippery incline. They showed the dual nature of the slip length, i.e., a stabilizing effect far away from criticality but a destabilizing effect near criticality. The gravity-driven film flow is influenced by the slip length and several studies [31–34] have been performed with the slip effects. Ding and Wong [35] investigated the dynamics of a thin Newtonian liquid film flowing along a heated slippery substrate. They used both the weighted-residual model and a Benney-type model to discuss the influence of slip length. They found that, for small slip length, the weighted-residual model is more reasonable than the Benney-type model. Later, Ellaban *et al.* [36] studied the stability of a binary liquid film flowing down a uniformly heated slippery incline. Their main conclusion was that both the bottom slip and thermocapillary destabilize the flow. Recently, Chattopadhyay *et al.* [37] investigated the thermocapillary instability on a Newtonian film flowing along a nonuniformly heated slippery incline, using the classical long-wave expansion technique. They concluded that the influence of the thermocapillary force amplifies the destabilizing nature of the slip length. In addition, they discussed the existence of a transcritical Hopf bifurcation provided the slip length satisfies a certain condition. Very recently, Chattopadhyay *et al.* [38] reported a detailed comparative study on the stability of a viscoelastic liquid flowing down a slippery inclined plane. They considered both the weighted-residual model and a Benney-type model to discuss the impact of the slip length. They found that the weighted-residual model is more reasonable than the Benney-type model when the slip length is small. However, both the models are well accepted when the slip length is moderate.

The study of viscoelastic fluid flow has become important in the last few decades due to its drag-reduction property [39]. Viscoelastic fluids are widely used to characterize the lubrication behavior of bearings and gears. Therefore, under various physical flow conditions, the instabilities of such flows must be explored thoroughly. Pal and Samanta [40] and later Chattopadhyay *et al.* [38] studied the influence of the wall slip when a viscoelastic fluid (Walter's liquid B″) flows along a slippery inclined plane. Both of these studies showed the destabilizing effect of the slip length on the surface mode in the long-wave regime for the viscoelastic liquid. On the other hand, we know that, for nonisothermal flows, thermocapillarity has a significant impact on interfacial instability. The studies of interfacial heat transfer and stability of thin liquid films have a variety of applications in engineering and science. In several industrial equipments, such as falling film evaporators, condensers, etc., thin liquid films are extensively used because of their small thermal resistance and large contact area. Apart from these, thin liquid films are also used for the thermal protection in rocket engines and to cool microelectronic devices. The surface-wave instabilities are extremely injurious to increase the glossy texture of a product. Therefore it is desirable to suppress the obstructive factors so that one can develop the exact conditions for homogeneous growth of the thin liquid for various industrial applications. Sadiq and Usha [41] considered the flow of a thin layer of viscoelastic fluid (Walter's liquid B″) flowing down a nonuniformly heated inclined plane where they investigated only the linear stability. Sarma and Mondal [42] investigated the Marangoni instability in a thin layer of viscoelastic fluid (Maxwell viscoelastic model) where they additionally discussed the experimental possibilities regarding the occurrence of Marangoni instability in a viscoelastic liquid layer.

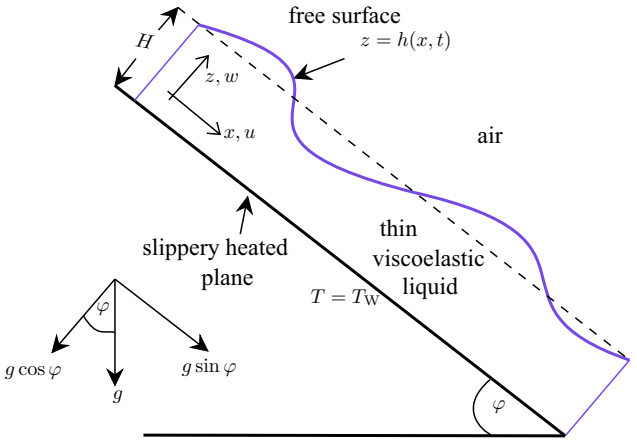

FIG. 1. Schematic representation of thin viscoelastic liquid flow down a heated slippery slope.

However, for a thin viscoelastic film (Walter's liquid B′) flowing down a slippery inclined plane, it remains unknown how the heating affects the stability of the system. Nowadays, viscoelastic liquids are widely used as the working media in various engineering applications, encompassing microfluidic systems. For instance, the chemical and nuclear industries, bioengineering, geophysics, and so on. Walter's B′ type finds relevance and importance in chemical technology, medicinal diagnosis, and petroleum industries. The above mentioned studies [38,40–42] motivate us to pursue a study on the Marangoni instability in a thin viscoelastic liquid to understand the influence of the rheological behavior of the liquid on the stability and dynamics of the system. Specifically, we extend the study of Chattopadhyay *et al.* [38] by accounting the bottom heating. Both analytical and numerical methods have been utilized to better understand how the complicated interplay between heating, strong surface tension, viscoelasticity, and bottom slip affect the stability of the flow.

The contents of this paper are organized as follows. In Sec. II, we formulate the mathematical problem. In Sec. III, a linear stability analysis is performed for the associated Orr-Sommerfeld eigenvalue problem. We construct an equation for the free surface using the long-wave expansion technique in Sec. IV. We then carry out a weakly nonlinear stability analysis of the system in Sec. V. The numerical simulations of the nonlinear evolution equation are investigated in Sec. VI. We draw our conclusions in Sec. VII.

II. MATHEMATICAL DESCRIPTION

We consider the gravity-driven two-dimensional laminar flow of an incompressible, thin, weakly viscoelastic liquid film over a uniformly heated slippery substrate inclined at an angle φ with the horizon. Here we consider the rheological model of the viscoelastic liquid in the layer is the Walter's B′ liquid. A schematic representation of the film flow is shown in Fig. 1. An (x, z) coordinate is chosen with the x axis pointing along the incline and the z axis pointing into the liquid layer. The interfacial surface of the wavy thin film may be expressed as $z = h(x, t)$, where h denotes the thickness of the film at any instant t. The temperature of the inclined plane is maintained at a constant value denoted by $T_W > T_\infty$, where T_∞ is the ambient air temperature which is assumed to remain motionless. The liquid film is assumed to be nonvolatile and the dynamic influence of the ambient air is also neglected.

The proposed model represents an approximation to the first-order in elasticity and obeys constitutive equation of state given by Beard and Walters [17] as

$$\tau_{ij} = -p\delta_{ij} + 2\mu e_{ij} - 2\gamma_0 \frac{\delta e_{ij}}{\delta t}, \tag{1a}$$

where τ_{ij} is the stress tensor, p is the isotropic pressure, δ_{ij} is the Kronecker delta, γ_0 is the viscoelastic coefficient, $e_{ij} = (\partial_i u_j + \partial_j u_i)/2$ is the rate of strain tensor. The corotational derivative of the rate of strain tensor $\delta e_{ij}/\delta t$ is defined as

$$\frac{\delta e_{ij}}{\delta t} = \partial_t e_{ij} + u_m \partial_m e_{ij} - \partial_m u_j e_{im} - \partial_m u_i e_{mj}, \quad m = x, z. \tag{1b}$$

For the rest of the study, we assume the velocity components of the viscoelastic liquid as $u_x = u$, $u_z = w$ to adjust with the usual notations. The constitutive equation (1a) recovers the Newtonian case when we set the viscoelastic coefficient γ_0 to zero. As an example of Walter's liquid B″, we may consider a certain mixture of polymethyl methacrylate in pyridine with density $0.98 \times 10^3\ \mathrm{kg\,m^{-3}}$, viscosity $0.79\ \mathrm{N\,s\,m^{-2}}$ and viscoelastic coefficient $\gamma_0 = 0.04\ \mathrm{N\,s^2\,m^{-2}}$ [40,43].

The governing equations for the liquid film are obtained from the two-dimensional conservation of mass, momentum and energy equations which are represented in vector form as

$$\nabla \cdot \mathbf{U} = 0, \tag{2}$$

$$\rho(\mathbf{U}_t + (\mathbf{U} \cdot \nabla)\mathbf{U}) = \rho \mathbf{g} + \nabla \cdot \tau, \tag{3}$$

$$T_t + (\mathbf{U} \cdot \nabla)T = \kappa \nabla^2 T, \tag{4}$$

where $\nabla = (\partial_x, 0, \partial_z)$ is the gradient operator, $\mathbf{U} = (u, 0, w)$ denotes the velocity vector, ρ is the density of the liquid, $\mathbf{g} = (g \sin\varphi, 0, -g\cos\varphi)$ is the gravitational acceleration, T is the absolute temperature of the liquid and κ is the thermal diffusivity. The elements of the Cauchy stress tensor τ are given in (1a) and (1b).

The boundary conditions at the interface with the slippery substrate ($z = 0$) are the Navier slip condition and no-penetration condition, which are as follows:

$$u = \beta_s \partial_z u, \quad w = 0, \tag{5}$$

where β_s is the dimensional slip coefficient and $\beta_s = 0$ leads back to the default no-slip condition. For instance, Voronov and Papavassiliou [31] experimentally measured the value of slip length for different slippery substrates and found that the slip length for a polydimethylsiloxane slippery plane is of about 250 μm. One can find the proper range of slip length for various slippery substrates in Refs. [31,44].

Finally, since the substrate is maintained at a fixed temperature T_W, the thermal boundary condition at $z = 0$ is

$$T = T_W. \tag{6}$$

The boundary conditions at the free surface $z = h(x, t)$ are the balance of tangential and normal stresses and kinematic condition along with the Newton's law of cooling, which are as follows:

$$\mathbf{n} \cdot \tau \cdot \mathbf{t} = \nabla\sigma \cdot \mathbf{t}, \tag{7}$$

$$p_\infty + \mathbf{n} \cdot \tau \cdot \mathbf{n} = -\sigma \nabla \cdot \mathbf{n}, \tag{8}$$

$$\partial_t h + \mathbf{U} \cdot \nabla(h - z) = 0, \tag{9}$$

$$\lambda \nabla T \cdot \mathbf{n} + \alpha(T - T_\infty) = 0, \tag{10}$$

where $\mathbf{n}$ and $\mathbf{t}$ are the outward-directed unit normal and unit tangent vector at any point on the interface, respectively, σ is the surface tension, p_∞ denotes the atmospheric pressure, λ (>0) is the thermal conductivity, and α is the heat transfer coefficient.

It is also assumed that all the fluid properties remain constant throughout the study except the surface tension σ. The surface tension is assumed to depend linearly on the temperature as [45–47]

$$\sigma = \sigma_\infty - \sigma_t(T - T_\infty), \tag{11}$$

where σ_∞ is the surface tension of the liquid at $T = T_\infty$ and $\sigma_t = -d\sigma/dT(> 0)$ is the surface tension constant. However, there are some special cases such as water-alcohol solutions where the surface tension increases with the increasing value of the temperature [3].

Here we made an assumption that the evaporation is negligible and fluid properties are constant except for the surface tension. To substantiate this fact we would like to highlight an experimental example of this fact for aqueous solutions of ethanol, as reported by Khattab *et al.* [48]. According to them, for a mixture that is approximately 17% ethanol, at a temperature of 293 K, the viscosity is $\mu = 2.62 \times 10^{-3}$ Pa s, the density is $\rho = 9.47 \times 10^2$ kg m^{-3} and the rate of change in surface tension with temperature can be estimated to be $\sigma_t \approx 9 \times 10^{-5}$ N K^{-1} m^{-1}. From the data presented by Khattab *et al.*, Ellaban *et al.* [36] calculated the temperature difference $\Delta T = 2.18 \times 10^{-3}$ K and also deduced the rates of change in viscosity and density and mentioned that, for the specified temperature difference, the resulting scaled variations in viscosity and density are of the order 10^{-5}, which is very small to consider the approximation that density and viscosity are temperature independent.

The elements of the Cauchy stress tensor τ obtained from (1a) and (1b) are presented as

$$\tau_{xx} = -p + 2\mu\partial_x u - 2\gamma_0\{\partial_{xt}u + u\partial_{xx}u + w\partial_{xz}u - 2(\partial_x u)^2 - \partial_z u(\partial_z u + \partial_x w)\}, \tag{12a}$$

$$\tau_{zz} = -p + 2\mu\partial_z w - 2\gamma_0\{\partial_{zt}w + w\partial_{zz}w + u\partial_{xz}w - 2(\partial_z w)^2 - \partial_x w(\partial_z u + \partial_x w)\}, \tag{12b}$$

$$\tau_{xz} = \tau_{zx} = \mu(\partial_z u + \partial_x w) - \gamma_0\{\partial_{zt}u + \partial_{xt}w + u(\partial_{xx}w + \partial_{xz}u) + w(\partial_{xz}w + \partial_{zz}u) - 2(\partial_z u\partial_z w + \partial_x u\partial_x w)\}. \tag{12c}$$

The governing equations and boundary conditions are made nondimensional and the dimensionless variables marked by an asterisk in the superscript are defined as

$$x = \mathcal{L}x^*, \quad (z, h) = H(z^*, h^*), \quad t = (\mathcal{L}/\mathcal{V})t^*, \quad u = \mathcal{V}u^*, \quad w = (\mathcal{V}H/\mathcal{L})w^*, \quad p = \rho\mathcal{V}^2 p^*,$$
$$T = T_\infty + T^*\Delta T, \quad (\tau_{xx}, \tau_{zz}) = \mu(\mathcal{V}/\mathcal{L})(\tau^*_{xx}, \tau^*_{zz}), \quad (\tau_{xz}, \tau_{zx}) = \mu(\mathcal{V}/H)(\tau^*_{xz}, \tau^*_{zx}), \tag{13}$$

where the longitudinal length scale $\mathcal{L}$ (associated with the characteristic wavelength on the free surface and of the same order as that of the wavelength) and the mean film thickness H are adopted as the length scales along the x and z axes, respectively, $\mathcal{V} = gH^2 \sin\varphi/3\nu$ the characteristic velocity, $\nu = \mu/\rho$ is the kinematic viscosity and $\Delta T = T_W - T_\infty$.

Using the dimensionless variables above, the governing equations and the boundary conditions can be rendered in the following dimensionless form after removing the asterisk as follows:

(i) Governing equations:

$$\partial_x u + \partial_z w = 0, \tag{14}$$

$$\epsilon\mathrm{Re}(\partial_t u + u\partial_x u + w\partial_z u) = 3 + (\epsilon^2\partial_x\tau_{xx} + \partial_z\tau_{xz}), \tag{15}$$

$$\epsilon^2\mathrm{Re}(\partial_t w + u\partial_x w + w\partial_z w) = -3\cot\varphi + \epsilon(\partial_x\tau_{zx} + \partial_z\tau_{zz}), \tag{16}$$

$$\epsilon\mathrm{RePr}(\partial_t T + u\partial_x T + w\partial_z T) = \epsilon^2\partial_{xx}T + \partial_{zz}T. \tag{17}$$

(ii) Boundary conditions along the slippery inclined plane $z = 0$:

$$u = \beta\partial_z u, \quad w = 0, \tag{18}$$

$$T = 1, \tag{19}$$

where $\beta = \beta_s/H$ is the dimensionless slip length.

(iii) Boundary conditions on the free surface $z = h(x, t)$:

$$\mathcal{G}\tau_{xz} + \epsilon^2(\tau_{zz} - \tau_{xx})\partial_x h = -\epsilon \mathrm{Ma}(\partial_x T + \partial_x h \partial_z T)\mathcal{F}, \tag{20}$$

$$\overline{p}_\infty + \epsilon \mathrm{Re}^{-1}[\epsilon^2 \tau_{xx}(\partial_x h)^2 - 2\tau_{zx}\partial_x h + \tau_{zz}]\mathcal{F}^{-2} = \epsilon^2(\mathrm{We} - \mathrm{MaRe}^{-1}T)\partial_{xx}h\mathcal{F}^{-3}, \tag{21}$$

$$w = \partial_t h + u\partial_x h, \tag{22}$$

$$\partial_z T - \epsilon^2 \partial_x T \partial_x h = -\mathrm{Bi}\mathcal{F}T, \tag{23}$$

where $0 < \epsilon = H/\mathcal{L}$ ($\ll 1$) is the aspect ratio, $\mathrm{Re} = \mathcal{V}H/\nu$ is the Reynolds number, $\mathrm{Pr} = \nu/\kappa$ is the Prandtl number, $\mathrm{Ma} = \sigma_t \Delta T/(\mu\mathcal{V})$ is the Marangoni number, $\mathrm{We} = \sigma_\infty/(\rho\mathcal{V}^2 H)$ is the Weber number, and $\mathrm{Bi} = \alpha H/\lambda$ is the Biot number. We define $\mathcal{G} = [1 - \epsilon^2(\partial_x h)^2]$, $\mathcal{F} = [1 + \epsilon^2(\partial_x h)^2]^{1/2}$ and $\overline{p}_\infty = p_\infty/(\rho\mathcal{V}^2)$.

The dimensionless forms of the component of stress tensor are as follows:

$$\tau_{xx} = -\epsilon^{-1}\mathrm{Re}p + 2\partial_x u - 2\epsilon\mathrm{Re}\gamma\{\partial_{xt}u + u\partial_{xx}u + w\partial_{xz}u - 2(\partial_x u)^2 - \partial_z u(\epsilon^{-2}\partial_z u + \partial_x w)\}, \tag{24a}$$

$$\tau_{zz} = -\epsilon^{-1}\mathrm{Re}p + 2\partial_z w - 2\epsilon\mathrm{Re}\gamma\{\partial_{zt}w + w\partial_{zz}w + u\partial_{xz}w - 2(\partial_z w)^2 - \partial_x w(\partial_z u + \epsilon^2\partial_x w)\}, \tag{24b}$$

$$\tau_{xz} = \tau_{zx} = (\partial_z u + \epsilon^2\partial_x w) - \epsilon\mathrm{Re}\gamma\{\partial_{zt}u + \epsilon^2\partial_{xt}w + u(\epsilon^2\partial_{xx}w + \partial_{xz}u) + w(\epsilon^2\partial_{xz}w + \partial_{zz}u) - 2\partial_z u\partial_z w - 2\epsilon^2\partial_x u\partial_x w\}, \tag{24c}$$

where $\gamma = \gamma_0/(\rho H^2)$ is the dimensionless viscoelastic parameter.

III. BASE STATE AND LINEAR STABILITY ANALYSIS

The ϵ dependency is removed from (14)–(23) through the transformations $(\partial_x, \partial_t) \to \epsilon^{-1}(\partial_x, \partial_t)$ and $w \to \epsilon^{-1}w$. Consider a flat film solution of (14)–(23) with a constant film thickness $h = 1$ corresponding to a stationary flow. Setting all derivatives with respect to x and t to zero one easily obtains the solution of the base equations (14)–(23) as

$$\mathcal{U}(z) = 3\left\{(z + \beta) - \frac{z^2}{2}\right\}, \quad \mathcal{W}(z) = 0, \quad \mathcal{P}(z) = \overline{p}_\infty + \frac{3}{\mathrm{Re}}\cot\varphi(1 - z),$$
$$\Theta(z) = 1 - \frac{\mathrm{Bi}}{(1 + \mathrm{Bi})}z. \tag{25}$$

Equation (25) shows that the base flow velocity is explicitly dependent on the slip length β but is independent of the viscoelastic parameter γ. We also observe that the base flow temperature is dependent on the Biot number Bi. Note that the base flow velocity is a parabolic function of z while the base flow temperature is a linear function of z.

To conduct a linear stability analysis, the perturbed equilibrium solution of the ϵ independent rescaled equations are expressed as follows:

$$h = 1 + \eta(x, t), \quad u = \mathcal{U}(z) + \widetilde{u}(x, z, t), \quad w = \widetilde{w}(x, z, t),$$
$$p = \mathcal{P}(z) + \widetilde{p}(x, z, t), \quad T = \Theta(z) + \widetilde{T}(x, z, t), \tag{26}$$

where the tildes denote the added infinitesimal perturbations.

Let us search the solution of the perturbation equations in the normal-mode form as

$$(\widetilde{u}, \widetilde{w}, \widetilde{p}, \widetilde{T}, \eta) = (\widehat{u}(z), \widehat{w}(z), \widehat{p}(z), \widehat{T}(z), \widehat{\eta})\exp[ik(x - \omega t)], \tag{27}$$

where the "hat" quantities represent the amplitudes of the perturbation variables, k represents the perturbation wave number which is taken to be real and positive, and ω denotes a complex quantity whose real part gives the phase speed of the perturbation.

To simplify the analysis, the stream function ϕ is introduced as follows:

$$\phi = \Phi(z)\exp[ik(x-\omega t)], \tag{28}$$

and therefore the components of the velocity perturbation $\widetilde{u} = \partial_z\phi$, $\widetilde{w} = -\partial_x\phi$ becomes $\widehat{u} = \mathcal{D}\Phi$, $\widehat{w} = -ik\Phi$. Here "$\mathcal{D}$" denotes the differentiation with respect to the z operator. Following Refs. [36,40], the following Orr-Sommerfeld-type (OS) ordinary differential equations are obtained over the domain $0 < z < 1$ as follows:

(i) Governing equations:

$$[1-ik\gamma\mathrm{Re}(\mathcal{U}-\omega)]\mathcal{D}^4\Phi - [(1-2k^2\gamma)ik\mathrm{Re}(\mathcal{U}-\omega)+2k^2]\mathcal{D}^2\Phi + [k^4+(1-k^2\gamma)ik^3\mathrm{Re}(\mathcal{U}-\omega)-3ik\mathrm{Re}]\Phi = 0, \tag{29}$$

$$(\mathcal{D}^2-k^2)\widehat{T} - ik\mathrm{RePr}\left[(\mathcal{U}-\omega)\widehat{T} + \frac{\mathrm{Bi}}{1+\mathrm{Bi}}\Phi\right] = 0. \tag{30}$$

(ii) Boundary conditions on $z = 0$:

$$\mathcal{D}\Phi = \beta\mathcal{D}^2\Phi, \quad \Phi = 0, \quad \widehat{T} = 0. \tag{31}$$

(iii) Boundary conditions at the undeformed film surface $z = 1$:

$$[1-ik\gamma\mathrm{Re}(\mathcal{U}-\omega)](\mathcal{D}^2+k^2)\Phi + ik\mathrm{Ma}\left(\widehat{T} - \frac{\mathrm{Bi}}{1+\mathrm{Bi}}\widehat{\eta}\right) - 3(\widehat{\eta}+ik\gamma\mathrm{Re}\Phi) = 0, \tag{32}$$

$$[1-ik\gamma\mathrm{Re}(\mathcal{U}-\omega)]\mathcal{D}^3\Phi - [3k^2-3ik\gamma\mathrm{Re}+(1-3k^2\gamma)ik\mathrm{Re}(\mathcal{U}-\omega)]\mathcal{D}\Phi - ik\left[3\cot\varphi + k^2\left(\mathrm{ReWe} - \frac{\mathrm{Ma}}{1+\mathrm{Bi}}\right)\right]\widehat{\eta} = 0, \tag{33}$$

$$(\mathcal{U}-\omega)\widehat{\eta} + \Phi = 0, \tag{34}$$

$$(\mathcal{D}+\mathrm{Bi})\widehat{T} - \frac{\mathrm{Bi}^2}{1+\mathrm{Bi}}\widehat{\eta} = 0. \tag{35}$$

It is observed in absence of the viscoelastic parameter γ, the above Orr-Sommerfeld type boundary-value problem (29)–(35) reduces to that obtained by Pascal [36]. The above equations (29)–(35) form an eigenvalue problem where ω is the eigenvalue. The solution of the eigenvalue problem (29)–(35) can be obtained in terms of long-wavelength asymptotic analysis as

$$[\Phi, \widehat{\eta}, \widehat{T}, \omega] = [\Phi^{(0)}, \eta^{(0)}, \widehat{T}^{(0)}, \omega^{(0)}] + ik[\Phi^{(1)}, \eta^{(1)}, \widehat{T}^{(1)}, \omega^{(1)}] + O(k^2). \tag{36}$$

Substituting the above expansion (36) into the system of equations (29)–(35) and assuming that the flow parameters Re, Pr, Ma, k^2We, Bi, and γ are of order unity, we obtain a hierarchy of problems at different orders of k. Given that the first-order term of the phase speed $ik\omega^{(1)}$ is imaginary, the term $k^2\omega^{(1)}$ contributes to the growth rate of the instability. Here we would like to highlight that the Weber number We appearing in the normal stress boundary condition (33) has a stabilizing influence and helps to prevent the breakup of the nonlinear wave phenomenon and due to this fact, in the subsequent discussion, the Weber number We is assumed to be of order $O(1/k^2)$.

To find the solutions of the undetermined quantities at different orders of k, without loss of generality the eigenvalue problem and be normalized and set $\widehat{\eta}^{(0)} = 1$ and $\widehat{\eta}^{(1)} = \widehat{\eta}^{(2)} = 0$. Substitution of (36) into (29)–(35) results in

(i) Leading-order equations:

(a) Governing equations:

$$\mathcal{D}^4\Phi^{(0)} = 0, \ \mathcal{D}^2\widehat{T}^{(0)} = 0. \tag{37}$$

(b) Boundary conditions on $z = 0$:

$$\mathcal{D}\Phi^{(0)} = \beta\mathcal{D}^2\Phi^{(0)},\ \Phi^{(0)} = 0,\ \widehat{T}^{(0)} = 0. \tag{38}$$

(c) Boundary conditions at the undeformed film surface $z = 1$:

$$\mathcal{D}^2\Phi^{(0)} - 3 = 0, \quad \mathcal{D}^3\Phi^{(0)} = 0, \tag{39}$$

$$\mathcal{U} - \omega^{(0)} + \Phi^{(0)} = 0, \quad (\mathcal{D} + \mathrm{Bi})\widehat{T}^{(0)} - \frac{\mathrm{Bi}^2}{1+\mathrm{Bi}} = 0. \tag{40}$$

(ii) Leading-order solutions:

$$\Phi^{(0)} = \frac{3}{2}z^2 + 3\beta z, \quad \omega^{(0)} = 3(1+2\beta), \quad \widehat{T}^{(0)} = \frac{\mathrm{Bi}^2}{(1+\mathrm{Bi})^2}z. \tag{41}$$

Observe that both $\Phi^{(0)}$ and $\omega^{(0)}$ is free from γ but affected by β.

(iii) First-order equations:

(a) Governing equations:

$$\mathcal{D}^4\Phi^{(1)} - \gamma\mathrm{Re}(\mathcal{U} - \omega^{(0)})\mathcal{D}^4\Phi^{(0)} - \mathrm{Re}(\mathcal{U} - \omega^{(0)})\mathcal{D}^2\Phi^{(0)} - 3\mathrm{Re}\Phi^{(0)} = 0, \tag{42}$$

$$\mathcal{D}^2\widehat{T}^{(1)} - \mathrm{RePr}\left[(\mathcal{U} - \omega^{(0)})\widehat{T}^{(0)} + \frac{\mathrm{Bi}}{1+\mathrm{Bi}}\Phi^{(0)}\right] = 0. \tag{43}$$

(b) Boundary conditions on $z = 0$:

$$\mathcal{D}\Phi^{(1)} = \beta\mathcal{D}^2\Phi^{(1)}, \quad \Phi^{(1)} = 0, \quad \widehat{T}^{(1)} = 0. \tag{44}$$

(c) Boundary conditions at the undeformed film surface $z = 1$:

$$\mathcal{D}^2\Phi^{(1)} - \gamma\mathrm{Re}(\mathcal{U} - \omega^{(0)})\mathcal{D}^2\Phi^{(0)} - 3\gamma\mathrm{Re}\Phi^{(0)} + \mathrm{Ma}\left(\widehat{T}^{(0)} - \frac{\mathrm{Bi}}{1+\mathrm{Bi}}\right) = 0, \tag{45}$$

$$\mathcal{D}^3\Phi^{(1)} - \gamma\mathrm{Re}(\mathcal{U} - \omega^{(0)})\mathcal{D}^3\Phi^{(0)} - \mathrm{Re}(\mathcal{U} - \omega^{(0)})\mathcal{D}\Phi^{(0)} + 3\gamma\mathrm{Re}\mathcal{D}\Phi^{(0)} - (3\cot\varphi + k^2\mathrm{ReWe}) = 0, \tag{46}$$

$$\Phi^{(1)} - \omega^{(1)} = 0, \quad (\mathcal{D} + \mathrm{Bi})\widehat{T}^{(1)} = 0. \tag{47}$$

(iv) First-order solutions:

$$\Phi^{(1)} = 9\mathrm{Re}(1+\beta)\left[\frac{z^5}{120} - \frac{z^4}{24} - \frac{\beta}{6}z^3 + \frac{(1+3\beta)}{6}z^2 + \frac{\beta(1+3\beta)}{3}z\right] + [3\cot\varphi + k^2\mathrm{ReWe} - 9\gamma\mathrm{Re}(1+\beta)]\left(\frac{z^3}{6} - \frac{z^2}{2} - \beta z\right) + \frac{\mathrm{MaBi}}{2(1+\mathrm{Bi})^2}(z^2 + 2\beta z), \tag{48}$$

$$\omega^{(1)} = \mathrm{Re}(1+\beta)\left\{\frac{6}{5} + 6\beta + 9\beta^2 + 3\gamma(1+3\beta)\right\} - \left(\frac{k^2}{3}\mathrm{ReWe} + \cot\varphi\right)(1+3\beta) + \frac{\mathrm{MaBi}}{2(1+\mathrm{Bi})^2}(1+2\beta). \tag{49}$$

From condition (47) we can see that $\omega^{(1)} = \Phi^{(1)}(1)$ and therefore the neutral stability relation is given by $\omega^{(1)} = 0$. Solving this for Re, we obtain the following expression for the critical Reynolds number for the surface mode in the limit $k \to 0$ as

$$\mathrm{Re}_c = \frac{15}{\mathcal{Y}}\left[\cot\varphi(1+3\beta) - \frac{\mathrm{MaBi}}{2(1+\mathrm{Bi})^2}(1+2\beta)\right], \tag{50a}$$

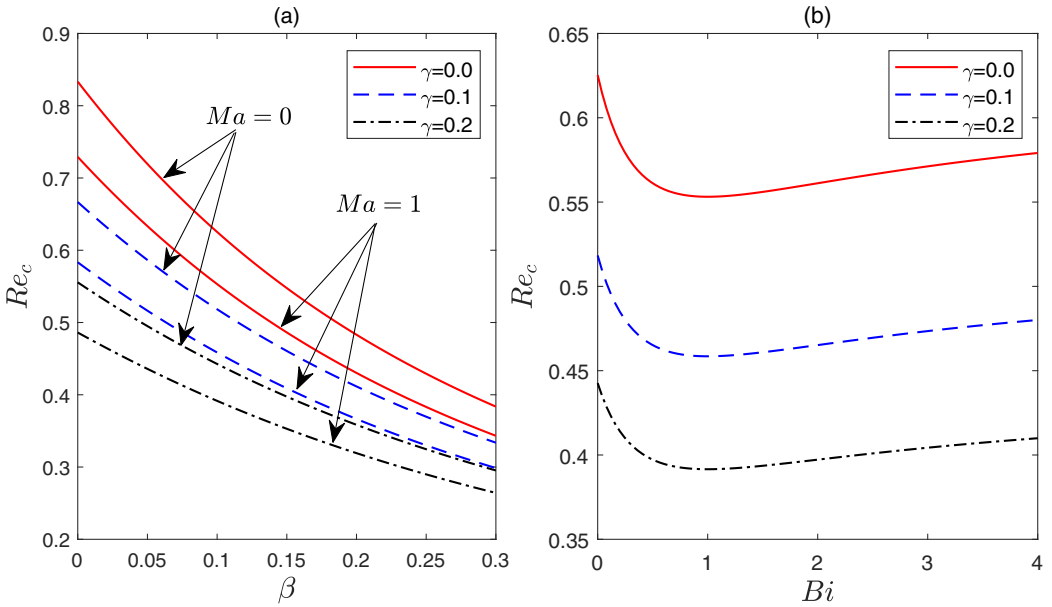

FIG. 2. Variation of the critical Reynolds number (Re_c) as a function of (a) slip length β (fixed Bi = 1), (b) Biot number Bi (fixed Ma = 1, $\beta = 0.1$) for the surface mode or H-mode when the viscoelastic parameter γ varies with $\varphi = \pi/4$.

where $\mathcal{Y} = 9(1+\beta)[(2+10\beta+15\beta^2)+5\gamma(1+3\beta)]$. This is the cutoff value of the Reynolds number after which the flow becomes linearly unstable. In the absence of γ, β, and Ma, the above relation reduces to $(5/6)\cot\varphi$ which exactly matches to that obtained by Benjamin [49] and Yih [50]. Furthermore, in an isothermal environment, Re_c is similar to the result of Pal and Samanta [40] in absence of surfactant. The slight dissimilarities appear in the expression of the Re_c due to choice of different scalings by Ref. [40].

In this investigation, we have considered that the liquid layer is thick enough so that inertial effects are relevant. The appropriate range would extend from tens of micrometers to about 1 mm [3]. Then, the resulting values for the scaled slip length β would range up to values of order 10^{-1} and this matches well with the range of Anjalaiah and Usha [51]. The same order of magnitude for slip length β applies when the substrate is composed of a porous material. In that case, the dimensioned slip length will be $\beta = \sqrt{\mathcal{P}}/B_\mathrm{J}$, where $\mathcal{P}$ is the permeability and B_J is the Beavers-Joseph constant. According to Beavers and Joseph [29], the value of B_J is from 0.1 to 4. According to Nield and Bejan [52], for common porous materials, $\sqrt{\mathcal{P}}$ extends from very small numbers to values comparable to 10^{-2} mm. Setting the mean film thickness $H = 2.4$ mm with $\sqrt{\mathcal{P}} = 8.58 \times 10^{-2}$ mm and allowing the Beavers-Joseph constant to range over the specified values, Sadiq *et al.* [47] considered the interval for the scaled slip length β from 0.0089 to 0.3575. The results that are discussed in the present study correspond to β values from 0 to 0.2.

If we consider the thickness of the mixture $H = 10^{-2}$ m with density 0.98×10^3 kg m^{-3} and viscoelastic coefficient $\gamma_0 = 0.04$ N s^2 m^{-2}, then $\gamma \approx 0.4$. Due to this, we have considered it in the range $\gamma \in [0-0.2]$ [41,53,54].

Figure 2(a) presents the variation of critical Reynolds number Re_c with the slip length β for different viscoelastic parameter γ. We observe that the Re_c reduces with the increasing value of β for a given γ in the presence or absence of thermocapillarity. This demonstrates the destabilizing effect of β. Furthermore, Re_c decreases with increasing γ, and this fact indicates the destabilizing effect of the viscoelastic parameter γ. Moreover, Re_c decreases in the presence of thermocapillarity.

This shows the destabilizing effect of thermocapillarity. Physically, the Marangoni number measures the variation in surface tension due to the temperature difference between the surroundings and the bottom surface, which indicates that the heating causes a variation in surface tension, and this results in a less stable flow. Since the surface tension increases as temperature decreases, the peaks of the disturbances will have higher surface tension because they are far from the bottom. Hence, the liquid is drawn toward the peaks, which causes the disturbances to grow, and therefore flow becomes unstable. Figure 2(b) shows how varying the Biot number Bi while holding the Marangoni number Ma and slip length β constant affects the stability of the flow. We observe that there is a specific value of the Biot number (Bi $= 1$) at which the flow is most unstable for a given viscoelastic parameter γ. We observe for a given γ, as the Bi increases from zero to one, the flow is destabilizing whereas, beyond that value as Bi increases, the critical Reynolds number increases, i.e., the flow is stabilizing beyond Bi $= 1$. This agrees with Fig. 2(b) which shows a minimum occurring at Bi $= 1$. Hence we can conclude that the Biot number plays a double role; for Bi < 1 it produces a destabilizing effect but for Bi > 1 it produces stabilization. Physically, the Biot number Bi is the ratio of heat transfer resistance inside the thin film to the free surface in the contact with the ambient air. When a constant thermal gradient is applied to the inclined plane which is greater than the temperature of the ambient air, the very small Biot number physically interprets that the heat conduction inside the liquid film is much faster than the heat convection away from its free surface. The case Bi $= 0$ corresponds to an insulating fluid layer or, in other words, the temperature will be uniform throughout the layer. On the other hand, the case Bi $\to \infty$ corresponds to an infinite rate of heat transfer across the interface, that is to say that the temperature of the interface will remain fixed at the ambient value. When Bi increases from zero, in the liquid layer a temperature distribution begins to develop. Now if the free surface is not a planar one, then the temperature along the free surface will be greater in the troughs than at the crests, which creates Marangoni stresses and hence destabilizes the flow. However, when Bi is large, the temperature along the free surface will approach the constant ambient medium and hence the thermocapillary force will be feeble. As a consequence, there exists an optimal value of the Biot number, Bi $= 1$, for which the thermocapillarity will be the maximum, and this results in a minimum value for Re_c.

Following Goussis and Kelley [7], we introduce the parameters χ, M^*, $\mathcal{B}$, and Ka as

$$\mathrm{Re} = \frac{2}{3}\chi \sin\varphi, \quad \mathrm{Ma} = \frac{3M^*}{2\chi^{2/3}\sin\varphi}, \quad \mathrm{Bi} = \mathcal{B}\chi^{1/3}, \quad \mathrm{We} = \frac{9\mathrm{Ka}}{2\chi^{5/3}\sin^2\varphi},$$

where

$$\chi = \frac{gH^3}{2\nu^2}, \quad M^* = \frac{\sigma_t \Delta T}{\rho}\left(\frac{2}{g\nu^4}\right)^{1/3}, \quad M = \frac{M^*\mathcal{B}\chi^{1/3}}{1+\mathcal{B}\chi^{1/3}}, \quad \mathcal{B} = \frac{\alpha}{\lambda}\left(\frac{2\nu^2}{g}\right)^{1/3}, \quad \mathrm{Ka} = \frac{\sigma_\infty}{\rho(4g\nu^4)^{1/3}}.$$

Note that the new flow parameters are implicitly dependent on the Reynolds number. In terms of these parameters, as $k \to 0$, the relation (50a) reduces to

$$(\chi \sin\varphi)^2 = \frac{45}{2\mathcal{Y}}\left[\chi\cos\varphi(1+3\beta) - \frac{3}{4}\frac{M\chi^{1/3}}{(1+\mathcal{B}\chi^{1/3})}(1+2\beta)\right]. \tag{50b}$$

There are various limits that can be taken from the equation (50b) and comparisons that can be drawn. For example, the viscoelastic and slip-free limit can be obtained by setting $\gamma = \beta = 0$, which yields

$$(\chi \sin\varphi)^2 = \frac{5}{4}\left[\chi\cos\varphi - \frac{3}{4}\frac{M\chi^{1/3}}{(1+\mathcal{B}\chi^{1/3})}\right]. \tag{50c}$$

The expression (50c) exactly recovers the dispersion relation obtained by Goussis and Kelley [7].

IV. LONG-WAVE APPROXIMATION

In this section, we construct a free-surface evolution equation in terms of the film thickness h. We consider that Re, Pr, Ma, ϵ^2We, Bi, and γ are of order unity. Since the long-wavelength modes are the most unstable ones for the film flow, we expand the physical quantities asymptotically in powers of ϵ ($\ll 1$) as $[u, w, p, T] = [u_0, w_0, p_0, T_0] + \epsilon[u_1, w_1, p_1, T_1] + O(\epsilon^2)$, where $[u_0, w_0, p_0, T_0]$ and $[u_1, w_1, p_1, T_1]$ represent the leading-order and first-order solutions, respectively. Substituting these expansions in (14)–(23) and collecting the coefficients of like powers of ϵ, the zeroth- and first-order equations are obtained and solved systematically. We obtain the leading-order velocity components, pressure, and temperature as

$$u_0 = 3\left(hz - \frac{z^2}{2} + \beta h\right), \tag{51}$$

$$w_0 = -3\left(\frac{z^2}{2} + \beta z\right)\partial_x h, \tag{52}$$

$$p_0 = \overline{p}_\infty - \epsilon^2 \mathrm{We}\partial_{xx} h + \frac{3\cot\varphi}{\mathrm{Re}}(h - z), \tag{53}$$

$$T_0 = 1 - \frac{\mathrm{Bi}z}{1 + \mathrm{Bi}h}. \tag{54}$$

We can see from the expression for equation (54) that the temperature at the free surface (i.e., at $z = h$) is $T^i = 1/(1 + \mathrm{Bi}h)$. This indicates that, in the adiabatic limit $\mathrm{Bi} \to 0$, the free-surface temperature $T^i = 1$ and in the case of free-surface equilibrium $\mathrm{Bi} \to \infty$, the interfacial temperature $T^i = 0$.

The solution of the first-order $O(\epsilon)$ stream-wise velocity component is given by

$$\begin{aligned} u_1 = \mathrm{Re}\Bigg[&\left\{\frac{3\cot\varphi}{\mathrm{Re}}\partial_x h - \epsilon^2\mathrm{We}\partial_{xxx} h - 9\gamma(\beta + h)\partial_x h\right\}\left(\frac{z^2}{2} - hz - \beta h\right) \\ &- 3\left\{\frac{\beta}{2}(z^2 - h^2) - \beta h(z + \beta) + \frac{z^3}{6} - \frac{h^2 z}{2}\right\}\left(\frac{h^2}{2} + \beta h\right)\partial_x h \\ &+ 9\left\{(\beta + h)\frac{z^4}{24} + (z^3 - h^3)\frac{\beta h}{6} + \frac{\beta^2 h z^2}{2} - \frac{h^4 z}{6} - (\beta + z)\left(\beta^2 h^2 + \frac{2}{3}\beta h^3\right)\right\}\partial_x h\Bigg] \\ &+ \frac{\mathrm{MaBi}}{(1 + \mathrm{Bi}h)^2}(\beta + z)\partial_x h. \end{aligned} \tag{55}$$

Substituting $u = u_0 + \epsilon u_1$ into the kinematic condition, which is written in the form of mass conservation as

$$\partial_t h + \partial_x \int_0^h (u_0 + \epsilon u_1) dz = 0, \tag{56}$$

we obtain the nonlinear evolution equation as

$$\partial_t h + \underbrace{A(h)\partial_x h}_{\text{(i)}} + \epsilon\partial_x\left[\underbrace{B(h)\partial_x h}_{\text{(ii)}} + \underbrace{\epsilon^2 C(h)\partial_{xxx} h}_{\text{(iii)}}\right] + O(\epsilon^2) = 0, \tag{57}$$

where

$$A(h) = 3(h^2 + 2\beta h),$$

$$B(h) = [3\mathrm{Re}\gamma(\beta + h) - \cot\varphi](h^3 + 3\beta h^2) + \mathrm{Re}\left(\frac{6}{5}h^6 + \frac{36}{5}\beta h^5 + 15\beta^2 h^4 + 9\beta^3 h^3\right) + \frac{\mathrm{MaBi}}{2(1 + \mathrm{Bi}h)^2}(h^2 + 2\beta h),$$

$$C(h) = \frac{1}{3}\mathrm{ReWe}(h^3 + 3\beta h^2).$$

Note that, by setting $\gamma = 0$, we exactly recover the evolution equation derived by Thiele *et al.* [55] for the corresponding one-sided model. Note that, their [55] modified Galileo number Γ, Ma, and $1/\mathrm{Bo}^*$ (where Bo is the Bond number) is same as our 3Re, MaRe, and $\epsilon^2\mathrm{ReWe}$. Here we explain different terms of the equation (57). Term (i) demonstrates that the surface waves are propagating downstream on a slippery plane. The first part of term (ii) indicates the influence of the viscoelastic parameter as well as the hydrostatic effect. The second part of term (ii) elucidates the destabilizing effects of the mean shear flow. The third part of the term (ii) describes the effect of thermocapillarity. Finally, the term (iii) expresses the stabilizing effects of the surface tension.

To study the linear stability, the flat film is disturbed with an infinitesimal perturbation. The film thickness h can be written as

$$h(x,t) = 1 + \eta(x,t), \tag{58}$$

where $\eta(x,t) \ll 1$ is an infinitesimal disturbance from the base solution at an instant t.

Using (58) in (57) with the transformations $(x,t) \to \epsilon(x,t)$ and retaining the terms up to the order $O(\eta^3)$ the evolution equation becomes

$$\eta_t + A\eta_x + B\eta_{xx} + C\eta_{xxxx} + A'\eta\eta_x + B'\left(\eta\eta_{xx} + \eta_x^2\right) + C'(\eta\eta_{xxxx} + \eta_x\eta_{xxx}) + \tfrac{1}{2}A''\eta^2\eta_x + B''\left(\tfrac{1}{2}\eta^2\eta_{xx} + \eta\eta_x^2\right) + C''\left(\tfrac{1}{2}\eta^2\eta_{xxxx} + \eta\eta_x\eta_{xxx}\right) + O(\eta^4) = 0, \tag{59}$$

where A, B, C and their corresponding derivatives are evaluated at $h = 1$.

Following a standard approach, we apply a normal-mode analysis and thus the disturbance η is expressed as

$$\eta = \Lambda \exp[i(kx - \omega t)] + \text{c.c.}, \tag{60}$$

where $\Lambda \ll 1$ is the amplitude of the infinitesimal disturbance, k is the wave number, $\omega = \omega_r + i\omega_i$ is the complex frequency, and c.c. is the complex conjugate of the term preceding it.

Substituting (60) in the linearized part of the equation (59), the dispersion relation is obtained as

$$D(\omega, k) = (Ck^2 - B)k^2 + i(Ak - \omega) = 0. \tag{61}$$

Equating the real and the imaginary parts of (61) results in

$$\omega_r = Ak \text{ and } \omega_i = Bk^2 - Ck^4. \tag{62}$$

The flow will be linearly stable or unstable if the linear growth rate $\omega_i < 0$ or $\omega_i > 0$, respectively. When $\omega_i = 0$, the flow is called neutrally stable. The neutral state $\omega_i = 0$ divides the (Re, k) plane into two separate regions, the linear stable region and the linear unstable region. For $\omega_i = 0$ the equation (62) yields

$$k = 0 \text{ and } k = \sqrt{\frac{B}{C}}, \tag{63}$$

which corresponds to two branches of the neutral curves and the flow is unstable between them. The wave number k_m with the maximum growth rate is obtained from the condition $d\omega_i/dk = 0$, which gives $k_m = k_c/\sqrt{2}$ where $k_c = \sqrt{B/C}$.

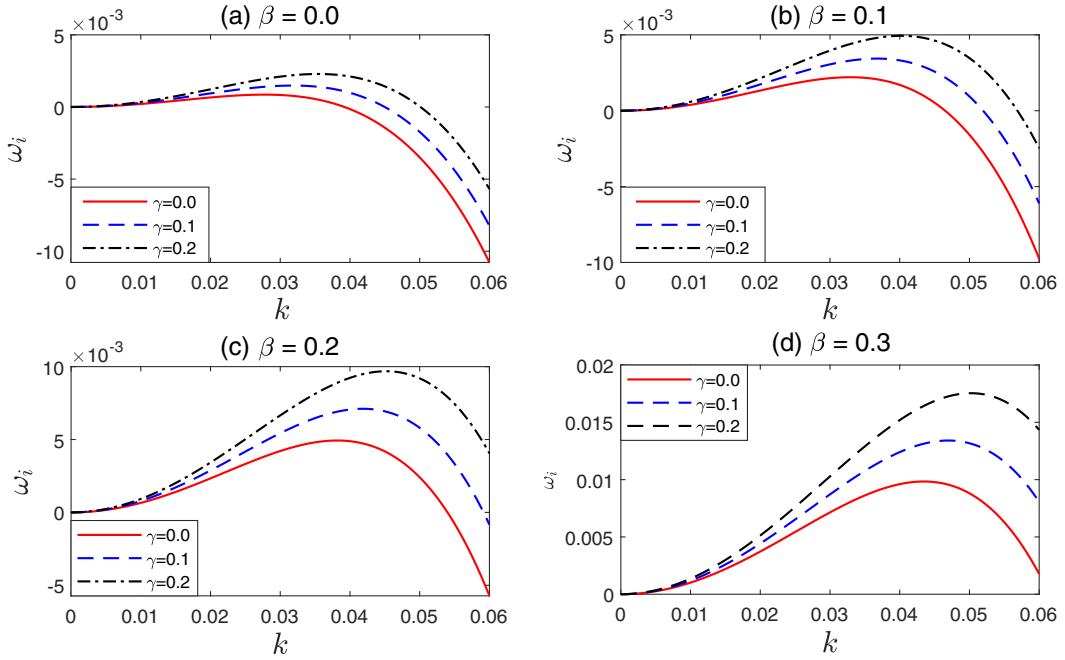

FIG. 3. The variation of the growth rate ω_i as a function of the wave number k for different slip length β and viscoelastic parameter γ with $\chi = 5$, Ka $= 3000$, $\mathcal{B} = 10$, $M = 20$, and $\varphi = \pi/4$.

In this paper, we shall not discuss the influence of surface tension, and the Kapitza number is fixed at Ka $= 3000$. In addition, we have also fixed the value of $\mathcal{B} = 10$. We choose the values of other flow parameters as $M \in [0, 80]$ and $\chi \in [0, 10]$.

Figure 3 displays the variation of the growth rate ω_i as a function of the wave number k for different values of the slip length β and viscoelastic parameter γ. We can see that, for a given γ and β, there always exists a cutoff wave number above which the growth rate of the disturbance amplitude decreases and below which it increases. We also observe that, for a fixed β, ω_i increases with increasing γ. This depicts the destabilizing nature of the viscoelastic parameter γ. In addition, we can observe that this destabilizing phenomenon enhances further with an increase in the slip length.

Figure 4 presents the variation of the growth rate ω_i as a function of wave number k for various values of Marangoni number M. We observe that, for a fixed $\gamma = 0.1$, ω_i increases with increasing M for a given slip length β. This confirms the destabilizing nature of the Marangoni number on the flow field. Furthermore, we can visualize that the growth rate increases more with an increment in γ $(= 0.2)$. This behavior again confirms the destabilizing role of the viscoelastic parameter γ.

Figure 5 demonstrates the neutral stability curves for the angle of inclination $\varphi = \pi/12$. We choose the other parameter values as $\gamma = 0$, $\mathcal{B} = 10$, and Ka $= 3000$. We can observe only one instability region above the neutral curve corresponding to the Marangoni number $M = 0$ for a given β. Figure 5(a) is plotted for $\beta = 0$. We have found only one neutral stability curve generated by the surface mode or H mode in (k, χ) plane when $M = 0$. As soon as M increases, the region of instability increases. We can see that, for $M \neq 0$, the region of instability increases, and two neutral stability curves emerge. Between these two curves, one appears in the low-Reynolds-number regime and is associated with the thermocapillary mode or S mode. The other one is associated with the H mode and it appears when the Reynolds number exceeds its critical value given in equation (50a). We can see that the onset of instability induced by the S mode and the onset of stability for the H mode remain on the χ axis when $M = 60$. Specifically, when the Reynolds number is very low,

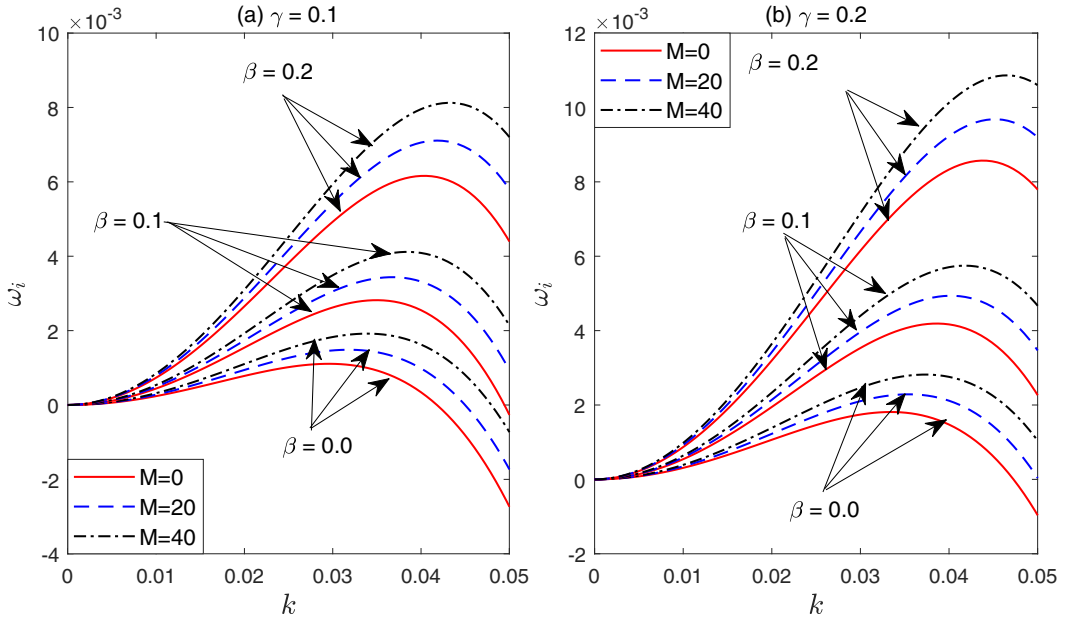

FIG. 4. The variation of the growth rate ω_i as a function of the wave number k for different Marangoni number M with $\chi = 5$, Ka $= 3000$, $\mathcal{B} = 10$, and $\varphi = \pi/4$.

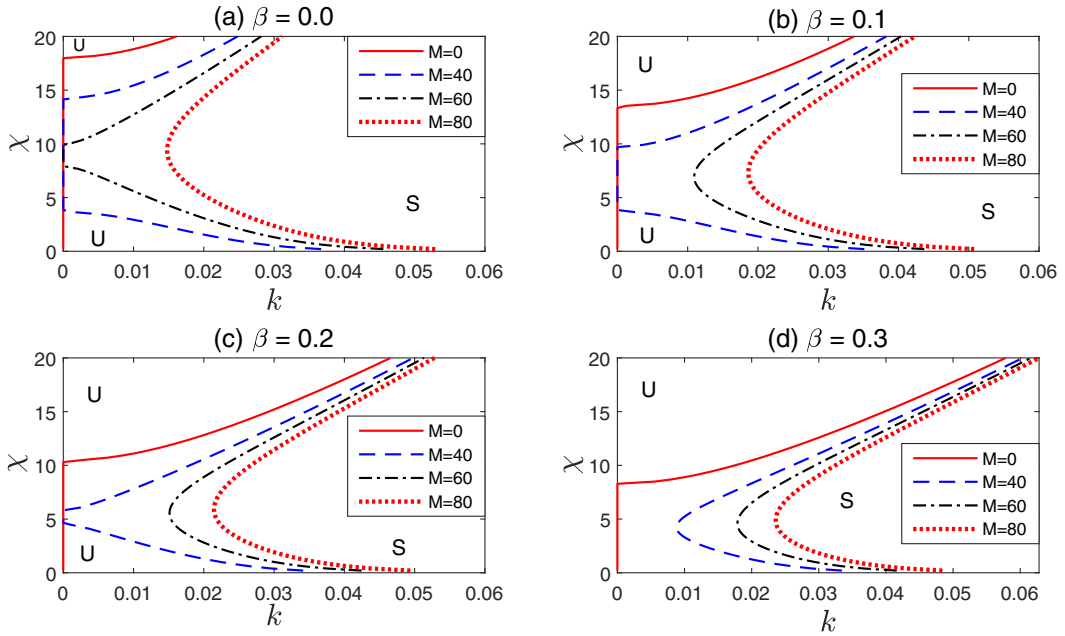

FIG. 5. Neutral stability curves for different Marangoni numbers M as a function of the wave number k with Ka $= 3000$, $\mathcal{B} = 10$, $\gamma = 0$, and $\varphi = \pi/12$. Here "S" and "U" indicate stable and unstable regions, respectively.

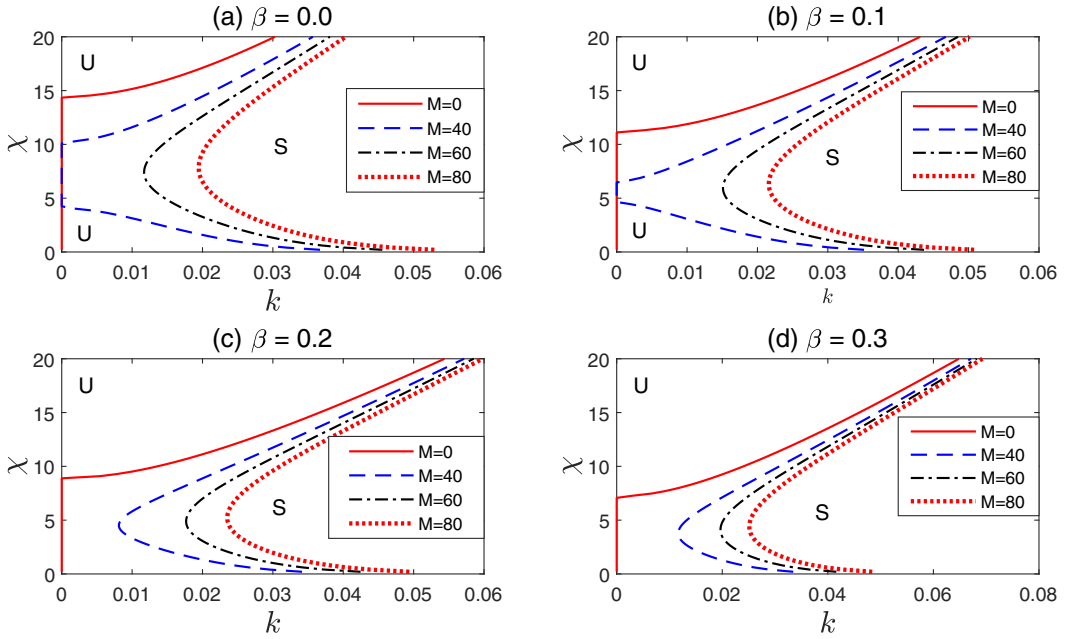

FIG. 6. Neutral stability curves for different Marangoni numbers M as a function of the wave number k with Ka $= 3000$, $\mathcal{B} = 10$, $\gamma = 0.1$, and $\varphi = \pi/12$. Here "S" and "U" indicate stable and unstable regions, respectively.

the S-mode instability appeared by the Marangoni stress emerges in the long-wave regime due to the infinitesimal perturbation of the temperature at the liquid surface. On the contrary, when the Reynolds number exceeds its threshold value, the H-mode instability arises due to the perturbation of the liquid surface in the long-wave regime. However, when χ increases, then the Reynolds number also increases, and therefore the inertia force increases which gradually dominates over the Marangoni force. Consequently, the S-mode instability becomes feeble and eventually dies down with increasing Re. Figure 5(a) further displays that with the increasing value of M, the two neutral stability curves merge with each other. We can see that, after a certain value of M, these two regions of instability threshold disappear and a nose-shape structure is found to develop where the tip of the nose intersects the χ axis at a certain $M = M^*$. When $M > M^*$, two neutral stability curves generate a single onset of stability. The results reveal the destabilizing influence of M. The parameter M, or equivalently the Marangoni number Ma measures the effect of thermocapillarity. Therefore, as it is increased, the temperature perturbations cause higher surface tension variation and thus destabilize the flow. A similar phenomenon of M is also observed in Figs. 5(b)–5(d). Comparing the cases corresponding to $\beta \neq 0$ with the no-slip case, we notice that, if the substrate is slippery, the unstable region increases significantly. On the contrary, in Fig. 6, we consider the case $\gamma \neq 0$. We choose $\gamma = 0.1$ here. A comparison between Figs. 5 and 6 clearly shows that the unstable region increases with increasing γ.

Physically, when the slip length increases, the velocity gradient at the bottom of the liquid layer reduces. Consequently, the friction of the liquid at the bottom diminishes which enhances the instability. On the other hand, the surface tension decreases with increasing temperature and the temperature is minimum in the trough and is maximum at the crest due to the difference in height of a perturbed liquid film surface. Here when the liquid is heated, the surface tension in the elevated region is larger compared with its neighboring depressed region because the liquid temperature at the crest of an elevation will be smaller than in the trough of a depression. When the Marangoni number increases, the temperature difference between the liquid and the ambient air also increases,

so the surface tension of the liquid decreases. Thus, the instability is reinforced when the substrate is heated.

V. WEAKLY NONLINEAR THEORY

In this section, we study the small-amplitude waves which develop immediately after the breakdown of the flat film solution $\eta = 0$. In the previous section, we investigated the linear stability analysis from which we obtained that, in the neutral state, all modes are neither stable nor unstable. The neutral state corresponds to $\omega_i = 0$ and the two branches of the neutral curve intersect at the bifurcation point $(\mathrm{Re}_c, 0)$. Thus, one expects in the vicinity of the upper branch of the neutral curve, a thin band of width $\xi \ll 1$ (say) of unstable modes around a central one appearing over a time $O(\xi^{-2})$ where $\omega_i \approx O(\xi^2)$. The main features of the system behavior can be obtained from an analysis of these modes and the nonlinear evolution of the unstable linear waves are investigated in the region where $\omega_i \approx O(\xi^2)$.

The above expectation, along with the anticipation that the wave packet may travel at a group velocity of order one, suggests a scale

$$x_1 = \xi x, \quad t_1 = \xi t, \quad t_2 = \xi^2 t, \ldots \tag{64}$$

for the multiple-scale analysis in developing a weakly nonlinear theory for the evolution of the envelope of a wave pattern at finite amplitude. Here, x, t are fast scales, whereas x_1, t_1, t_2 and so on are slow scales. It is assumed that these variables are mutually independent, so the temporal and spatial derivatives become

$$\partial_t \to \partial_t + \xi\partial_{t_1} + \xi^2\partial_{t_2} + \cdots \text{ and } \partial_x \to \partial_x + \xi\partial_{x_1} + \xi^2\partial_{x_2} + \cdots . \tag{65}$$

Now, the surface deformation will be expressed as

$$\eta(x, x_1, \ldots, t, t_1, t_2, \ldots) = \xi\eta_1 + \xi^2\eta_2 + \xi^3\eta_3 + \cdots . \tag{66}$$

Using (64)–(66) in equation (59) gives

$$(L_0 + \xi L_1 + \xi^2 L_2 + \cdots)(\xi\eta_1 + \xi^2\eta_2 + \xi^3\eta_3 + \cdots) = -\xi^2 N_2 - \xi^3 N_3 - \cdots , \tag{67}$$

where L_0, L_1, L_2 etc. are the operators and N_2, N_3 are the nonlinear terms that are given in the Appendix.

In the lowest order of ξ,

$$L_0\eta_1 = 0, \tag{68}$$

which has a solution of the form

$$\eta_1 = \Lambda(x_1, t_1, t_2)\exp[i\Theta] + \text{c.c.}, \tag{69}$$

where $\Theta = kx - \omega_r t$ and c.c. denotes the complex conjugate of the term preceding it. It should be noted here that the solution given in (69) is already obtained in connection with the linear stability analysis except ω is replaced by ω_r. This is because, in the vicinity of the neutral curve $\omega_i \approx O(\xi^2)$, the function $\exp(\omega_i t)$ is slowly varying and may be absorbed in $\Lambda(x_1, t_1, t_2)$.

In the second order, the perturbation system yields

$$L_0\eta_2 = -L_1\eta_1 - N_2. \tag{70}$$

Inserting (69) in (70) yields

$$L_0\eta_2 = -\left[\frac{\partial}{\partial t_1} + H_2\frac{\partial}{\partial x_1}\right]\Lambda\exp[i\Theta] + Q_1\Lambda^2\exp[2i\Theta] + \text{c.c.}, \tag{71}$$

where $H_2 = H_{2r} + iH_{2i} = A + 2ik(B - 2k^2C)$ and $Q_1 = Q_{1r} + iQ_{1i} = 2k^2(B' - C'k^2) - iA'k$, which is exactly the same form as obtained by Oron and Gottlieb [56]. The subscripts r and i denote the real and imaginary parts of the functions, respectively.

To determine η_2, we integrate (71). The uniformly valid solution for η_2 by eliminating secular (unbounded) terms, is obtained from the equation (71) as

$$\eta_2 = H_1 \Lambda^2 \exp[2i\Theta] + \text{c.c.}, \tag{72}$$

where $H_1 = Q_1/[4k^2(4Ck^2 - B)] = H_{1r} + iH_{1i}$. The same form is obtained by Mukhopadhyay and Chattopadhyay [45], Oron and Gottlieb [56], and Chattopadhyay [34,46].

Substituting the solutions η_1 and η_2 into (67) and using the solvability condition by eliminating its secular solution, the $O(\xi^3)$ equation related to the complex Ginzburg-Landau equation (CGLE) is obtained using *Mathematica* for the perturbation amplitude Λ as

$$\frac{\partial \Lambda}{\partial t_2} + i\mathcal{I}\frac{\partial \Lambda}{\partial x_1} + J_1 \frac{\partial^2 \Lambda}{\partial x_1^2} - \xi^{-2}\omega_i \Lambda + (J_2 + iJ_4)|\Lambda|^2 \Lambda = 0, \tag{73}$$

where

$$\left.\begin{aligned} \mathcal{I} = 2k(B - 2Ck^2)\xi^{-1} < 0, \quad J_1 = B - 6Ck^2, \\ J_2 = \frac{1}{2}(-B''k^2 + C''k^4) + \frac{(A')^2k^2 - 2(B'k^2 - 7C'k^4)(B'k^2 - C'k^4)}{16Ck^4 - 4Bk^2}, \\ J_4 = \frac{1}{2}A''k + \frac{A'k(B'k^2 - 7C'k^4) + 2A'k(B'k^2 - C'k^4)}{16Ck^4 - 4Bk^2}. \end{aligned}\right\} \tag{74}$$

Equation (73) and the values of the coefficients $\mathcal{I}$, J_1, J_2, J_4 coincide with the forms obtained by Oron & Gottlieb [56] and Chattopadhyay [34,46] in the case of the first-order Benney equation. The weakly nonlinear behavior of the film is investigated using (73). It is important to note that such an expansion is only valid for wave numbers close to neutral and not near-critical when ξ approaches zero. The solution of (73) for a filtered wave in which the spatial modulation does not exist and the diffusion term in (73) becomes zero is obtained by considering

$$\Lambda = a(t_2) \exp[-ib(t_2)t_2]. \tag{75}$$

This leads to a nonlinear ordinary differential equation for "a," namely,

$$\frac{\partial a}{\partial t_2} - ia\frac{\partial}{\partial t_2}[b(t_2)t_2] - a\xi^{-2}\omega_i + (J_2 + iJ_4)a^3 = 0, \tag{76}$$

where the real and imaginary parts, when separated from the above equation, yields

$$\frac{\partial a}{\partial t_2} = [\xi^{-2}\omega_i - J_2 a^2]a \tag{77a}$$

and

$$\frac{\partial [b(t_2)t_2]}{\partial t_2} = J_4 a^2. \tag{77b}$$

Equation (77a) is nothing but the Landau equation. This equation is used to characterize the nonlinear behavior of the traveling film flow. The second term on the right-hand side of equation (77a) is contributed by system nonlinearities. Equation (77b) is used to modify the wave speed induced by infinitesimal disturbance of system nonlinearities.

The threshold amplitude of the wave is obtained as

$$\xi a = \sqrt{\frac{\omega_i}{J_2}}, \tag{78}$$

and the nonlinear wave speed is then derived and given as

$$Nc_r = c_r + c_i \frac{J_4}{J_2}, \text{ where } c_r = \frac{\omega_r}{k}, \quad c_i = \frac{\omega_i}{k}. \tag{79}$$

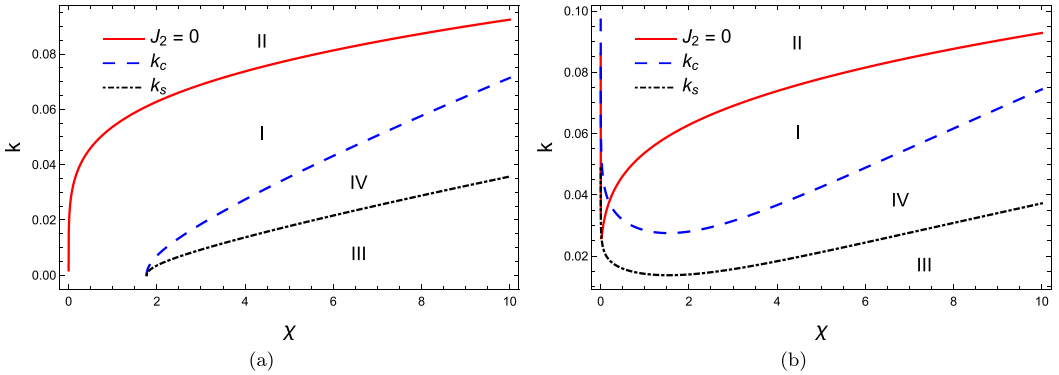

FIG. 7. Stability regions of nonlinear waves by weakly nonlinear stability analysis for (a) $M = 0$, (b) $M = 40$ with fixed $\beta = 0$, $\gamma = 0$, Ka $= 3000$, $\mathcal{B} = 10$, and $\varphi = \pi/4$. Zones I, II, III, IV denote the unconditional stable, subcritical unstable, explosive and supercritical stable regions, respectively.

Here the term J_2 is very important because, if J_2 becomes zero, then equation (77a) reduces to a linear partial differential equation (PDE) of the amplitude of the filtered wave. When $J_2 \neq 0$ the nonlinear stability depends on the sign of J_2. The sign of Landau coefficient J_2 determines the ultimate behavior of the system. Different zones [37,45,57] indicated in the graphs by I, II, III, and IV represent the following:

(i) Zone I: *Unconditional stable region*. In this region $\omega_i < 0$ and $J_2 > 0$, i.e., in this zone, finite-amplitude disturbances are unconditionally stable.

(ii) Zone II: *Subcritical unstable region*. In this region $\omega_i < 0$ and $J_2 < 0$. This zone indicates that, in the linear stable region, instability can be created by finite-amplitude disturbances.

(iii) Zone III: *Explosive region*. In this region $\omega_i > 0$ and $J_2 < 0$. This zone is always unstable for both the linear and weakly nonlinear cases.

(iv) Zone IV: *Supercritical stable region*. In this region $\omega_i > 0$ and $J_2 > 0$, i.e., in the linear unstable region, the disturbance will be supercritical stable.

Figures 7–9 describe the variation of the stable and unstable zones (I–IV) for different values of the Marangoni number ($M = 0, 40$), slip length ($\beta = 0, 0.2$), and viscoelastic parameter ($\gamma = 0, 0.2$). Figure 7 is plotted for $\beta = 0$ and $\gamma = 0$. Observing the variation of different zones of Fig. 7, it is found that the explosive zone (zone III) and supercritical stable zone (zone IV)

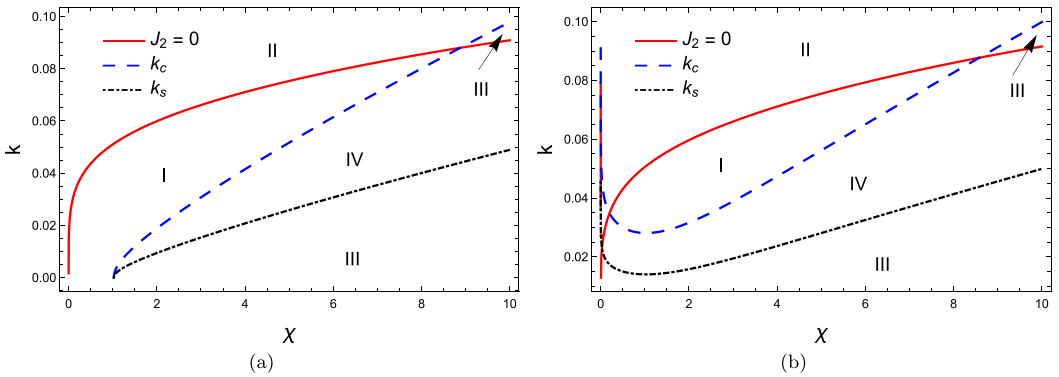

FIG. 8. Stability regions of nonlinear waves by weakly nonlinear stability analysis for (a) $M = 0$, (b) $M = 40$ with fixed $\beta = 0.2$, $\gamma = 0$, Ka $= 3000$, $\mathcal{B} = 10$, and $\varphi = \pi/4$. Zones I, II, III, IV denote the unconditional stable, subcritical unstable, explosive, and supercritical stable regions, respectively.

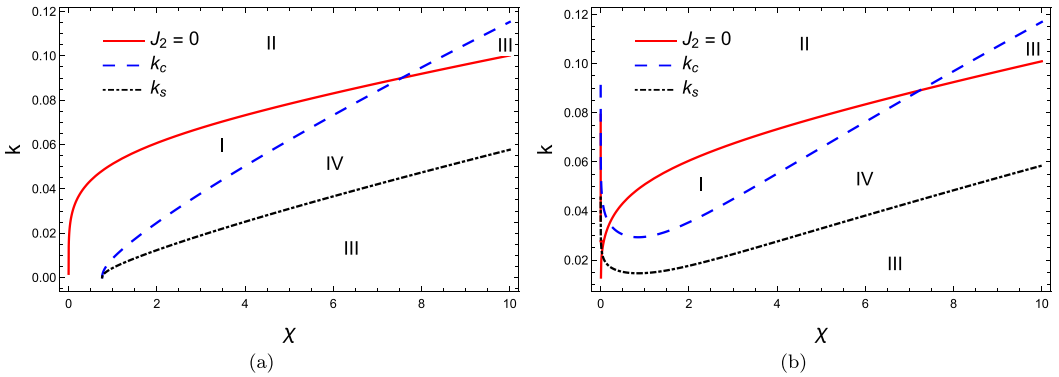

FIG. 9. Stability regions of nonlinear waves by weakly nonlinear stability analysis for (a) $M = 0$, (b) $M = 40$ with fixed $\beta = 0.2$, $\gamma = 0.2$, Ka $= 3000$, $\mathcal{B} = 10$, and $\varphi = \pi/4$. Zones I, II, III, IV denote the unconditional stable, subcritical unstable, explosive, and supercritical stable regions, respectively.

increase with increasing M in the range of the parameters considered. It is also observed that the band of unstable wave numbers also increases with increasing thermocapillarity. In other words, the Marangoni number has a destabilizing effect on the flow field. On the other hand, stability curves χ vs k in presence of the slip length ($\beta = 0.2$) are shown in Fig. 8. Comparing Figs. 7 and 8, it is observed that in presence of β, the explosive (zone III) and supercritical stable (zone IV) regions grow whereas the unconditional stable (zone I) and subcritical unstable (zone II) regions shrink. That is to say, the slip length β destabilizes the flow. Additionally, we can observe from Fig. 7(b) that, in the presence of thermocapillarity ($M \neq 0$), the curves corresponding to $J_2 = 0$ and $k = k_c$ intersect once; that is to say that the unconditional stable zone (zone I) is bounded below but unbounded above in our chosen parametric region. However, Fig. 8(b) shows that, when both thermocapillarity and slip are present ($M \neq 0$, $\beta \neq 0$), then the unconditional stable zone (zone I) becomes a bounded region. In Fig. 9, we investigate the effect of the viscoelastic parameter γ and for that we choose $\gamma = 0.2$. Scrutinizing Figs. 8 and 9, it is very clear that γ promotes the instability. In addition, we observe that when the capillary force at the free surface increases (Ka increases), the region of stability increases (figures are not presented here) for all values of β and γ. It is to be noted that the explosive state is mainly occurring at smaller wave numbers and higher values of χ.

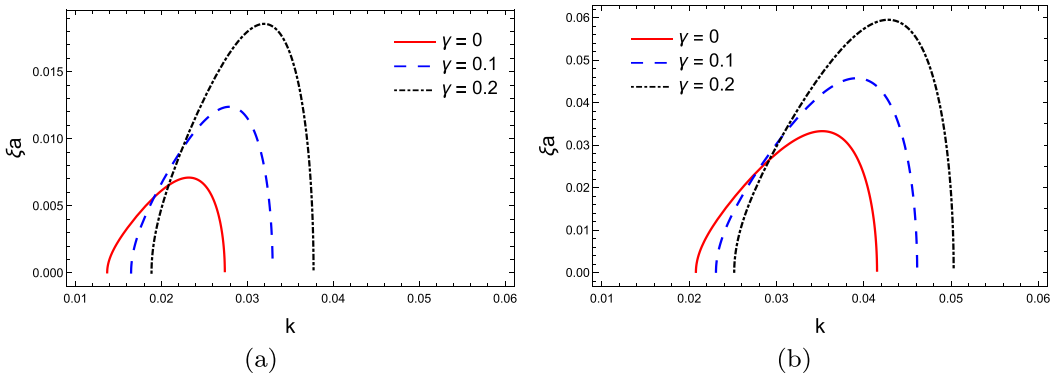

FIG. 10. Threshold amplitude ξa in supercritical stable region for (a) $\beta = 0$, (b) $\beta = 0.2$ with fixed $M = 0$, $\chi = 4$, Ka $= 3000$, $\mathcal{B} = 10$, and $\varphi = \pi/4$.

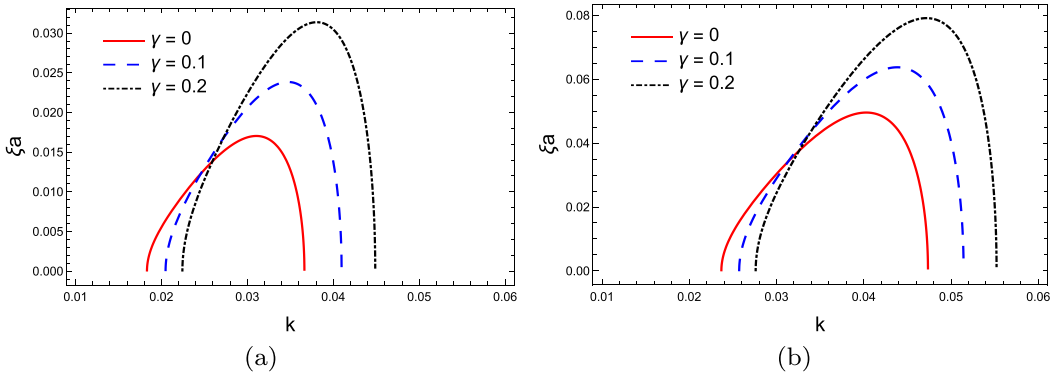

FIG. 11. Threshold amplitude ξa in supercritical stable region for (a) $\beta = 0$, (b) $\beta = 0.2$ with fixed $M = 40$, $\chi = 4$, Ka $= 3000$, $\mathcal{B} = 10$, and $\varphi = \pi/4$.

Figures 10 and 11 show the variation of the threshold amplitude ξa with wave number k in the supercritical stable zone for different values of viscoelastic parameter γ. All the figures show that the threshold amplitude becomes larger with an increase of γ in the absence or presence of β and this phenomenon enhances more in the presence of M. We can observe that there exists a critical wave number below which the threshold amplitude increases and above which it decreases. This phenomenon also confirms the stabilizing effect of odd viscosity. However, for any given μ, as the slip length increases, the threshold amplitude increases.

Figure 12 demonstrates the nonlinear wave speed of nonlinear waves for different Marangoni number M in the presence or absence of slip length and viscoelastic parameter. All the figures depict that for a small range of wave numbers, the wave speed initially increases, reaches a maximum, then decreases, and finally increases monotonically as a function of wave number. We further note that Nc_r increases with increasing β or γ for a fixed k.

The above weakly nonlinear analysis shows the existence of both a subcritical unstable region and a supercritical stable region for a film down a uniformly heated slippery inclined plane in the presence and absence of viscoelasticity. We also observe that there exists a value of $k_s = k_c/2$ such that when $k_s < k < k_c$ the flow is supercritically stable and the nonlinear equilibration occurs after the initial instability. The curve $k = k_s$ is obtained by equating the denominator of the second term of J_2 (which is $16Ck^4 - 4Bk^2$) to zero. We further notice that the curve $k = k_s$ divides the linearly unstable region into two portions where the nonlinear waves reach an explosive state (zone III) or attain a finite equilibrium amplitude (zone IV).

VI. NUMERICAL SIMULATIONS

To examine the growth of the film instability for a large time, we perform the numerical simulation consider of the full nonlinear evolution equation (57). Following Refs. [34,46,47,57,58], we impose the initial condition on the interface at $t = 0$,

$$h(x, 0) = 1 - 0.1 \cos\left(\frac{2\pi}{L}x\right). \tag{80}$$

We consider periodic boundary condition in space over the interval $[0, L]$, where L is the computational domain. Following Ding and Wong [35] and Chao *et al.* [59], we approximate the spatial solution of the equation (57) by the truncated Fourier series as

$$h(x, t) = \sum_{-N/2+1}^{N/2} \widehat{h}_n \exp\left(in\frac{2\pi}{L}x\right), \tag{81}$$

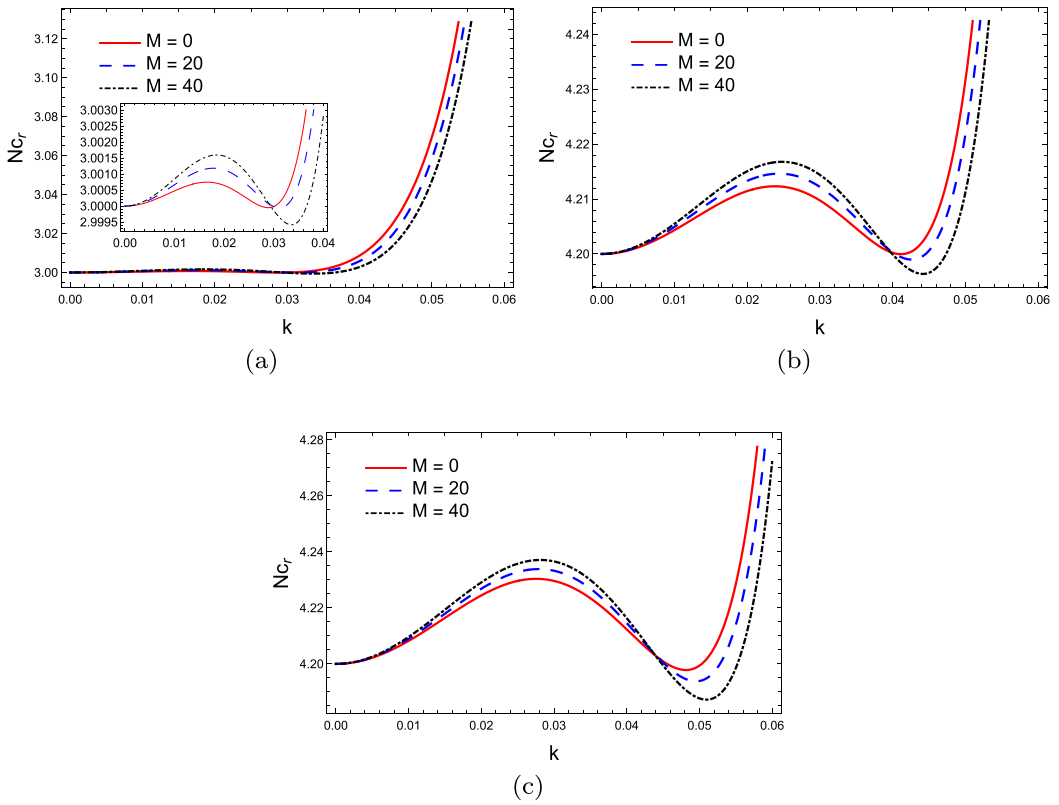

FIG. 12. Nonlinear wave speed as a function of wave number in supercritical stable region for different Marangoni number M when (a) $\beta = 0$, $\gamma = 0$; (b) $\beta = 0.2$, $\gamma = 0$; (c) $\beta = 0.2$, $\gamma = 0.2$ with fixed $\chi = 4$, Ka $= 3000$, $\mathcal{B} = 10$, and $\varphi = \pi/4$.

where $\widehat{h}_n$ is the Fourier amplitude of the disturbances. We substitute the expressions of h from (81) in (57) and obtain a system of nonlinear ODEs. We then time-integrate these system of nonlinear ODEs using the stiff-equation solver of MATLAB®. Chattopadhyay *et al.* [60] performed a space-time convergence study from where we conclude that $N = 2^8$ and the time step $\Delta t = 0.01$ are sufficient for our numerical simulations. In particular, we have reproduced the results of Ding and Wong [35] and Chao *et al.* [59]. For our subsequent discussion, we choose $N = 2^8$, $\Delta t = 0.01$, and the relative error tolerance as 10^{-6}. We have considered $L = 20\pi$ and $\epsilon = 0.1$ for the numerical discussion.

Moreover, following Refs. [35,59], we define an energy norm to measure the energy transfer from base flow into the disturbances in the following form:

$$E_2 = \frac{1}{L}\int_0^L h^2 dx. \tag{82}$$

Figure 13 presents typical curves corresponding to maximum ($h_{\max}$) and minimum ($h_{\min}$) film thickness for a long time in the absence of the slip length β. The top and the bottom panels are plotted for $\chi = 2$ and $\chi = 4$, respectively. It is found that the $h_{\max}$ and $h_{\min}$ increase with increasing viscoelastic parameter γ. We see that in the absence of the thermocapillary effect [Fig. 13(a)], $h_{\max}$ ($h_{\min}$) increases (decreases) up to a certain value, then monotonically decreases (increases) and ultimately tends to the basic state for a given γ. In Fig. 13(b), we consider $M = 40$ to capture the effect of the thermocapillarity. Comparing Fig. 13(a) with Fig. 13(b), we observe that the presence of the M increases the oscillatory nature of the time-dependent wave forms when $\gamma \neq 0$. In addition,

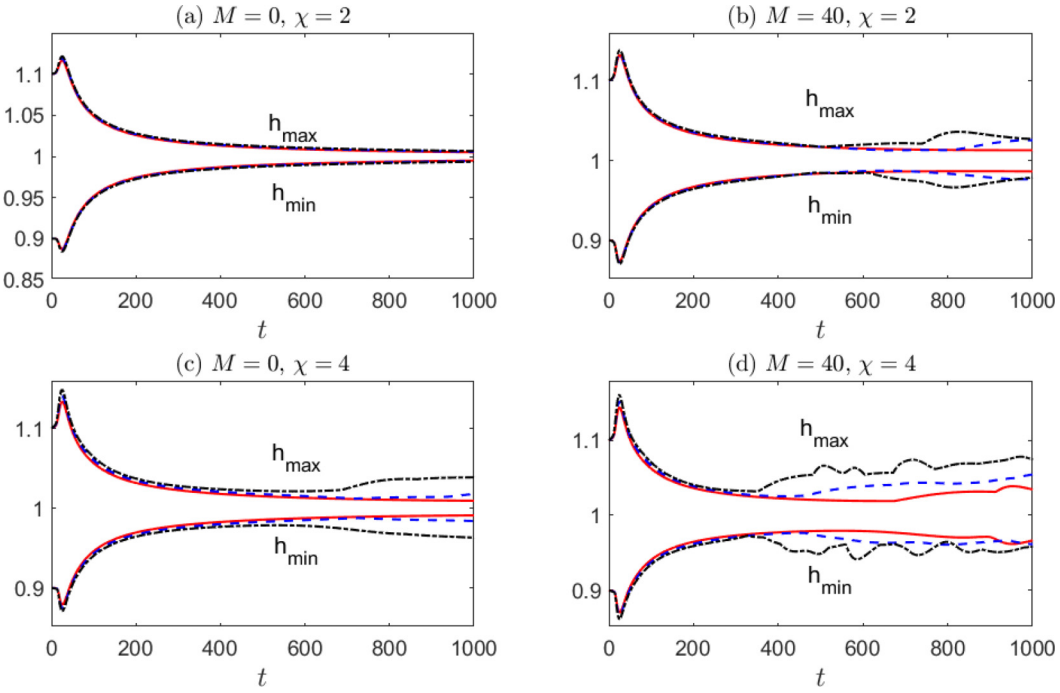

FIG. 13. Maximum (h_{max}) and minimum (h_{min}) amplitude of the film thickness for different viscoelastic parameters γ with $\beta = 0$, Ka $= 3000$, $\mathcal{B} = 10$, and $\varphi = \pi/4$. Here the solid lines (_____) is for $\gamma = 0$, dashed lines (_ _ _) indicate $\gamma = 0.1$, and dot-dashed lines (_ . _) represent $\gamma = 0.2$.

we can see that the saturation takes place at an earlier time with increase in M. Figures 13(c) and 13(d) show that, for $\gamma \neq 0$, the oscillations become more prominent with increase in χ.

Figure 14 displays the maximum (h_{max}) and minimum (h_{min}) film thickness of the thin viscoelastic film flowing down the inclined plane with wall slippage. Here we consider slip length $\beta = 0.1$ whereas the other parameters are same as Fig. 13. Here also we can see that the h_{max} (h_{min}) grows (decays) slightly from its initial value and then decays (rises) monotonically to an asymptotic limit. Comparing Figs. 13(a) and 13(b) with Figs. 14(a) and 14(b), it is found that, for $\chi = 2$, the effect of β is not much significant. However, for $\chi = 4$, the effect of higher slip length is very clear [Figs. 14(c) and 14(d)].

Figure 15 shows some free-surface configurations at a time instant $t = 200$ for different viscoelastic parameters γ corresponding to Figs. 13 and 14. Here we choose $\chi = 4$ and four different cases: (a) $M = 0$, $\beta = 0$; (b) $M \neq 0$, $\beta = 0$; (c) $M = 0$, $\beta \neq 0$, and (d) $M \neq 0$, $\beta \neq 0$. We observe that, for increasing γ, the growth rate is not significant in the absence of β and M [Fig. 15(a)]. Furthermore, in Fig. 15(b) we choose $M = 40$ and $\beta = 0$. Here also the growth rate is not very significant compared with Fig. 15(a). However, in absence of the thermocapillarity, if we take $\beta = 0.1$ [Fig. 15(c)], the growth rate is much more important than in Fig. 15(a). The distortion of the surface is conspicuous with increase in M when $\beta \neq 0$ [Fig. 15(d)]. In Figs. 15(a) and 15(b), it is observed that, in the absence of the slip length β, for a given γ, the amplitude of the wave diminishes after reaching a maximum and a one-hump solitary-like wave is formed. Furthermore, in the absence of the thermocapillarity, when $\beta = 0.1$, the amplitude of the one hump solitary-like wave increases eminently [Fig. 15(c)]. Finally, the Fig. 15(d) clearly portrays that the presence of both β and M amplifies the disturbances more.

Figure 16 describes the influence of the effect of the inertia on the thin-film flow in presence of the slip length β and Marangoni number M. In Fig. 16(a), we observe that for a given viscoelastic

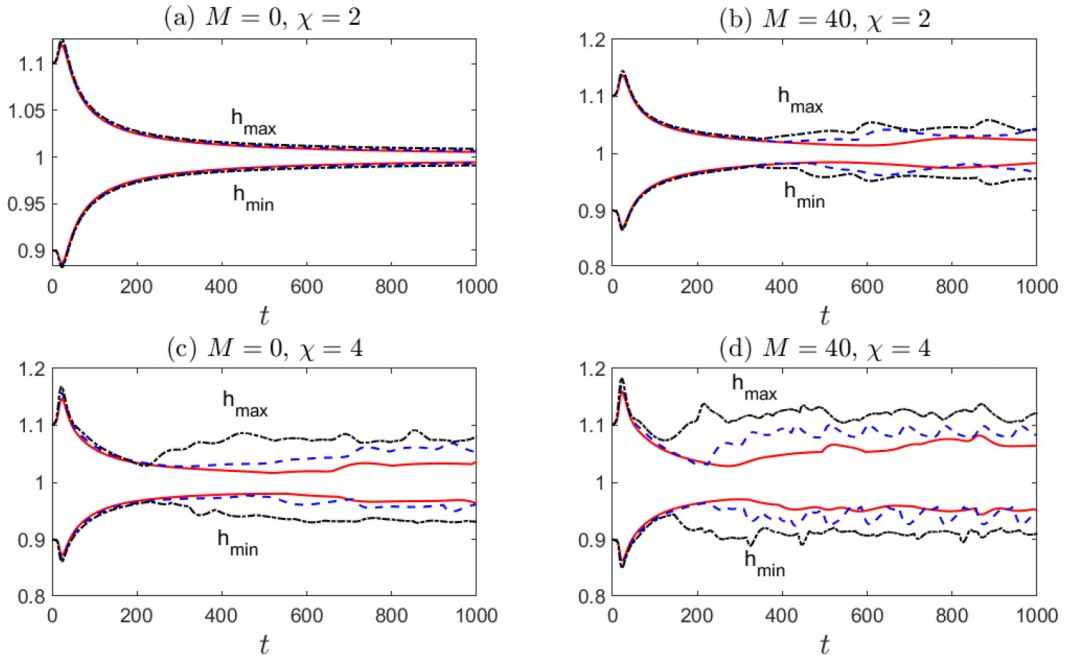

FIG. 14. Maximum ($h_{\max}$) and minimum ($h_{\min}$) amplitude of the film thickness for different viscoelastic parameters γ with $\beta = 0.1$, Ka $= 3000$, $\mathcal{B} = 10$. and $\varphi = \pi/4$. Here the solid lines (_____) is for $\gamma = 0$, dashed lines (_ _ _) indicate $\gamma = 0.1$ and dot-dashed lines (_ . _) represent $\gamma = 0.2$.

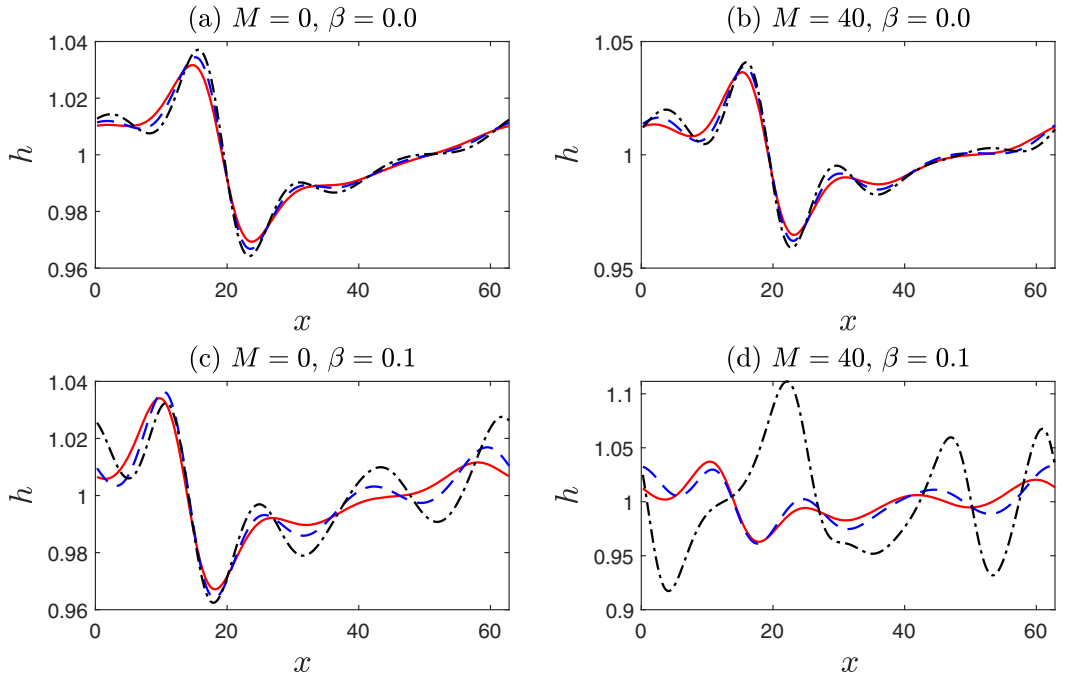

FIG. 15. Free-surface configuration at $t = 200$ for different viscoelastic parameters γ when Ka $= 3000$, $\chi = 4$, $\mathcal{B} = 10$, and $\varphi = \pi/4$. Here the solid lines (_____) is for $\gamma = 0$, dashed lines (_ _ _) indicate $\gamma = 0.1$, and dot-dashed lines (_ . _) represent $\gamma = 0.2$.

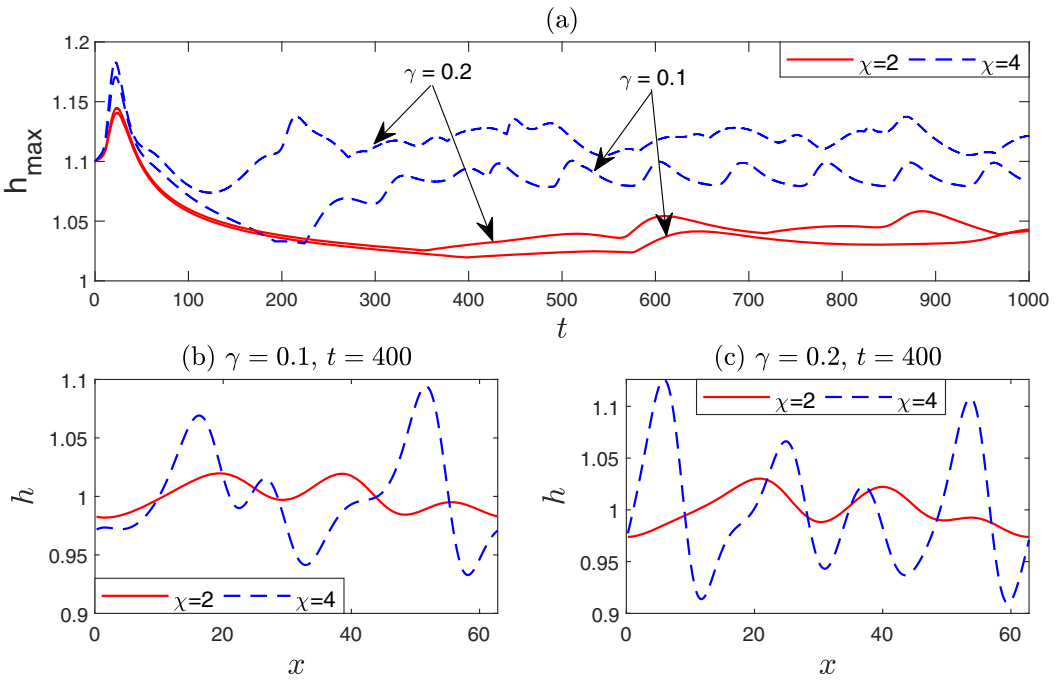

FIG. 16. Maximum amplitude and free-surface profiles of the film thickness for different viscoelastic parameter γ when $\beta = 0.1$, $M = 40$, Ka $= 3000$, $\mathcal{B} = 10$, and $\varphi = \pi/4$.

parameter γ, the crest of the wave enhances with an increase in Reynolds number. In all these cases, the disturbance amplitude grows slightly from its initial value and then starts to decay monotonically up to a certain time. The longtime waveforms are time-dependent modes that oscillate in the amplitude with an increase in Reynolds number for $\gamma = 0.1, 0.2$. We can see that for $\chi = 2$, up to $t < 350$ (approximately), the deviation of the $h_{\max}$ profiles is not very significant for an increment in γ. However, for $t > 350$, the deviation is clear. On the contrary, the $h_{\max}$ starts to deviate in a short time $t \approx 100$ for a given γ when $\chi = 4$. Figures 16(b) and 16(c) show the free-surface configurations at $t = 400$ corresponding to Fig. 16(a). In Fig. 16(b), we observe that for $\chi = 2$, the small amplitude wave gradually evolves with small humps whereas the interfacial waves possess higher humps for larger χ. Furthermore, comparing Figs. 16(b) and 16(c), we conclude that the instability of the thin liquid film is enhanced with increasing γ.

Figure 17 presents the maximum and minimum amplitude of the film thickness for different values of the slip length β. The left and right panels are plotted in the absence and presence of the Marangoni number M, respectively. First, we consider the effect of β without thermocapillary effect and viscoelasticity by setting $M = 0$, $\gamma = 0$ in Fig. 17(a). We observe that a larger slip length causes a steeper wave with a higher hump. This displays the destabilizing role of β on the flow field. Further we choose the values of γ as 0.1,0.2 in Figs. 17(c) and 17(e). It is found that the height of the hump is larger compared with the Newtonian film [Fig. 17(a)]. Furthermore, we note that in Fig. 17(a), for $\beta = 0.2$, the $h_{\max}$ starts to deviate from its basic state when $t > 250$ (approximately). When $\gamma = 0.1$, this nature of $\beta = 0.2$ is observed at $t > 50$ approx. However, when $\gamma = 0.2$, we can see this phenomenon even for $\beta = 0.1$. This clearly indicates the destabilizing behavior of the viscoelastic parameter γ in absence of the thermocapillarity. A comparison between the left and right panels shows that when the film is heated ($M \neq 0$), the height of the crest increases with the increase of the Marangoni number M.

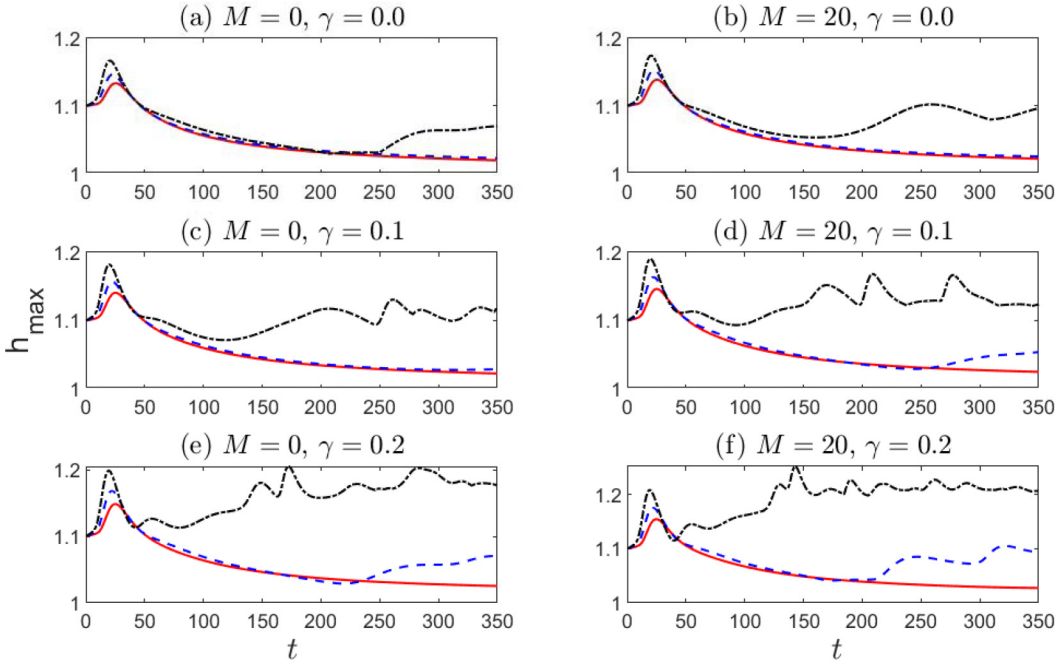

FIG. 17. Maximum amplitude of the film thickness h for different slip lengths β with $\chi = 4$, Ka $= 3000$, $\mathcal{B} = 10$, and $\varphi = \pi/4$. Here the solid lines (_____) is for $\beta = 0$, dashed lines (_ _ _) indicate $\beta = 0.1$, and dot-dashed lines (_ . _) represent $\beta = 0.2$.

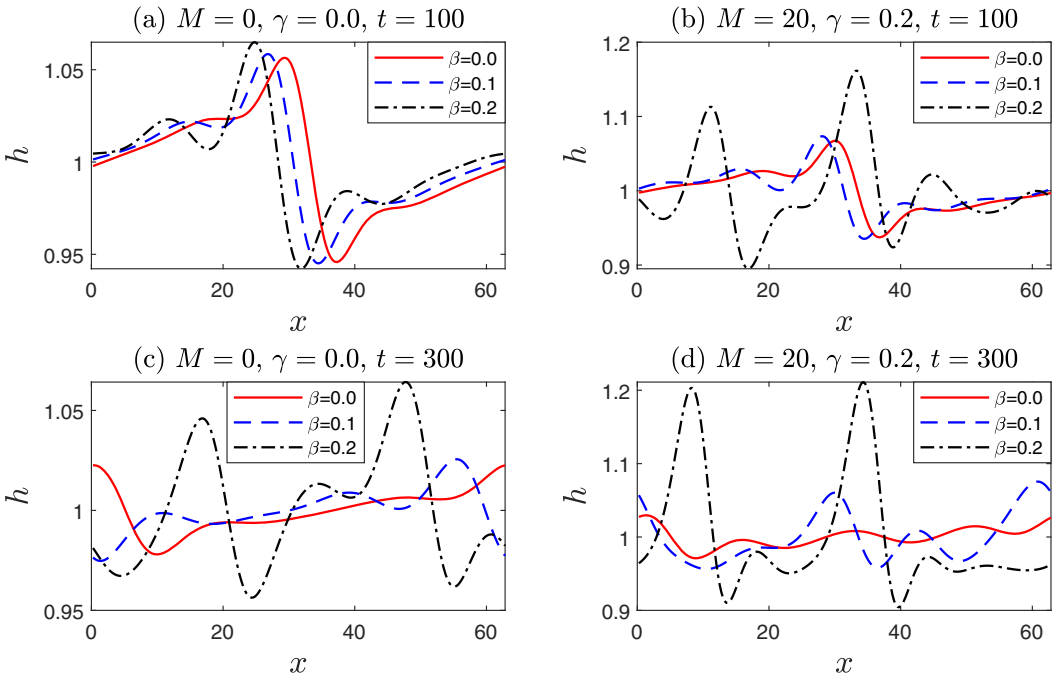

FIG. 18. Free-surface configuration for different vslip length β when Ka $= 3000$, $\chi = 4$, $\mathcal{B} = 10$, and $\varphi = \pi/4$.

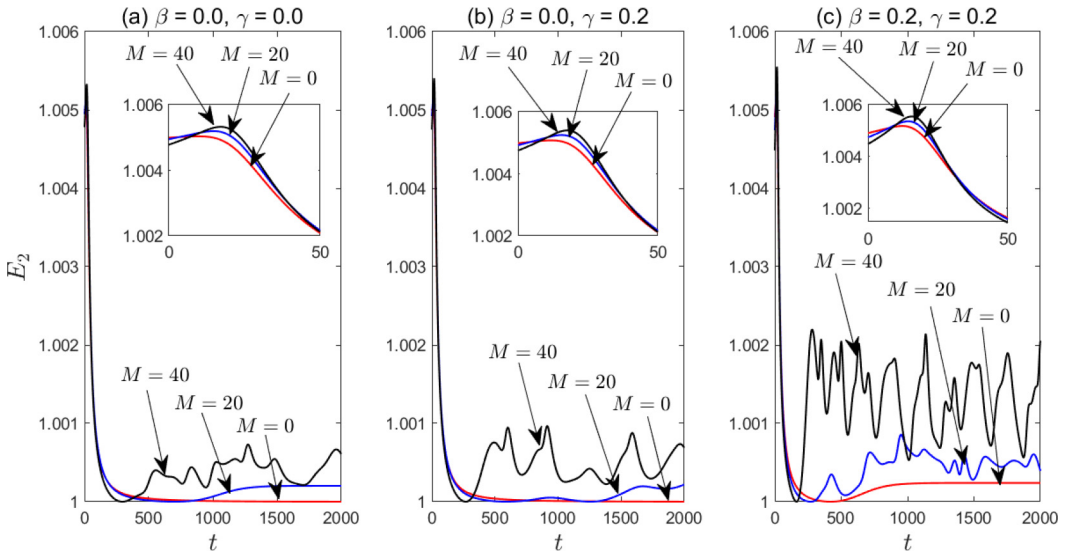

FIG. 19. Temporal evolution of the energy norm E_2. (a) $\beta = 0$, $\gamma = 0$; (b) $\beta = 0$, $\gamma = 0.2$; (c) $\beta = 0.2$, $\gamma = 0.2$ when $\chi = 1$, Ka $= 3000$, $\mathcal{B} = 10$, and $\varphi = \pi/2$.

Figure 18 displays the film thickness h when the disturbance waves evolve as a function of the stream-wise coordinate at two different time instants. The top panel is plotted for $t = 100$ whereas the bottom panel is plotted for $t = 300$. In Fig. 18(a), we observe that, in the absence of the Marangoni number M and viscoelastic parameter γ, the amplitude of the perturbations increases with increasing slip length β. This reveals the destabilizing mechanism of β. To characterize the effect of the thermocapillarity on the film instability, we set $M = 20$, $\gamma = 0.2$ in Fig. 18(b). We note that the instability is enhanced for a given β compared with the Newtonian isothermal case [Fig. 18(a)]. Figure 18(c) in the bottom panel describes that at time elapses, the amplitude of the perturbations enhances significantly for $\beta = 0.2$ compared with Fig. 18(a). Finally, Fig. 18(d) illustrates that in presence of both M and γ, the distortion of the surface is more prominent for a given β.

We explore the temporal evolution of the energy norm E_2 in a large timescale in Fig. 19 for three different Marangoni numbers M. In Fig. 19(a) we study the case when β and γ are both absent. In this case, we can see that the growth rate of E_2 increases with the increase of M. We find that the value of E_2 first increases at an early time ($t < 50$) and then decreases with time for a given M. We find that when there is no thermocapillarity, E_2 is always a steady-state after $t > 500$. For $M = 20$, the E_2 curve slightly increases at $t = 1000$ (approximately) and after $t > 1000$ the system evolves into a saturated steady-state with a constant-energy norm. However, for $M = 40$, we observe that for $t > 400$ (approximately), the value of energy norm E_2 significantly increases and then oscillates with time. Further in Fig. 19(b), we take $\gamma = 0.2$ to characterize the effect of the viscoelastic parameter γ on E_2. Comparing Figs. 19(a) with 19(b), we note that the viscoelastic parameter promotes the energy transfer from the base flow to the disturbance. In this case for $M = 0$, we cannot observe any significant change in the E_2 curve. When $M = 20$, we can see that the wave is oscillating and E_2 does not reach a steady state. Furthermore, for $M = 40$, no steady state is present, and the energy norm oscillates with time with a relatively large hump than $M = 40$ in Fig. 19(a). Figure 19(c) shows the evolution of the energy norm E_2 in presence of both β and γ. In this case when $M = 0$, the E_2 curve becomes steady after $t = 500$ approximately. However, for $M \neq 0$, the obtained E_2 curves demonstrate that a positive value of the Marangoni number enhances the instability after a short time.

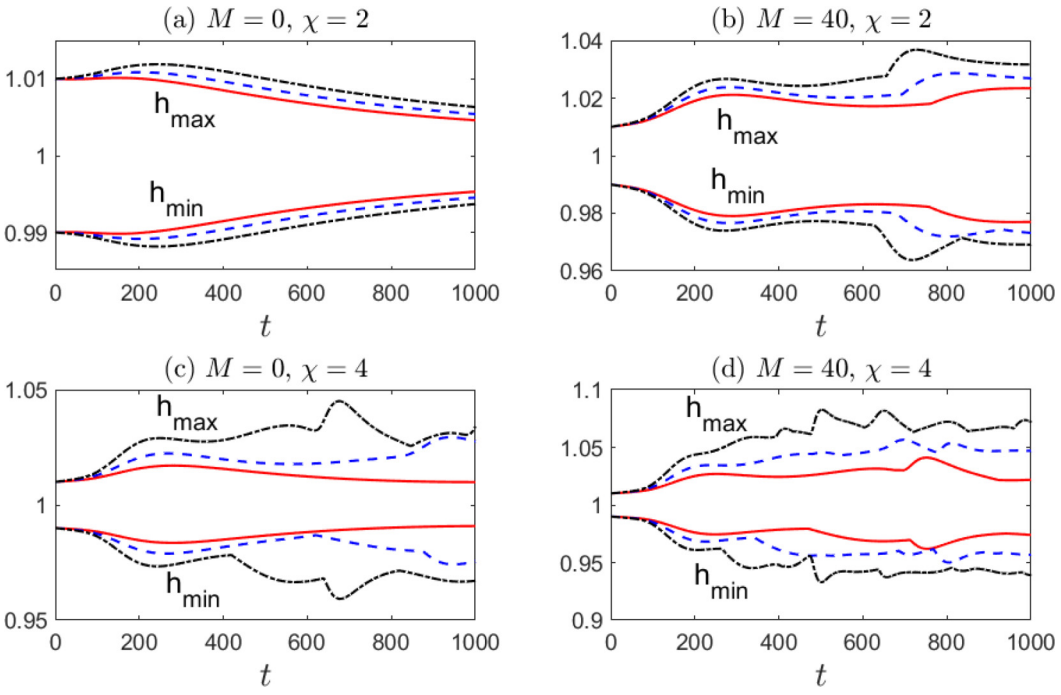

FIG. 20. Maximum ($h_{\max}$) and minimum ($h_{\min}$) amplitude of the film thickness [with initial profile equation (83)] for different viscoelastic parameters γ with $\beta = 0$, Ka $= 3000$, $\mathcal{B} = 10$, and $\varphi = \pi/4$. Here the solid lines (_____) is for $\gamma = 0$, dashed lines (_ _ _) indicate $\gamma = 0.1$, and dot-dashed lines ($- \cdot -$) represent $\gamma = 0.2$.

To investigate the effect of the smaller-amplitude perturbation, we impose the initial condition on the interface at $t = 0$,

$$h(x, 0) = 1 - 0.01 \cos\left(\frac{2\pi}{L}x\right), \tag{83}$$

where we choose the amplitude of the perturbation as 0.01 instead of 0.1. Figures 20–23 are plotted with the initial profile, given in equation (83).

Comparing Fig. 13 with Fig. 20, we can see that, when we consider a larger amplitude perturbation, the wave height decreases over a certain time span [see Fig. 13(d)], before the final surface waves develop, whereas this is not seen [see Fig. 20(d)] for smaller amplitude perturbation, except the cases when $M = 0$, $\chi = 2$ [see Fig. 20(a)] and $M = 0$, $\chi = 4$, $\gamma = 0$ [see Fig. 20(c)]. On the other hand, in presence of the slip length β also we find similar behavior. A comparison between Figs. 14 and 21 shows that, for larger amplitude, the wave height decreases up to a certain time, whereas for smaller amplitude the wave height decreases only when $M = 0$, $\chi = 2$ [see Fig. 21(a)]. Physically, when the perturbation amplitude is large, the nonsymmetrical wave forming quickly from the harmonic initial condition is dominated by (stabilizing) surface tension, which reduces the wave amplitude. Furthermore, the comparison of Figs. 16 and 22 with Figs. 17 and 23 also shows that for larger amplitude perturbation, the wave height initially increases, reaches its maximum, and then decreases up to a certain time, whereas for smaller amplitude perturbation the wave height always increases.

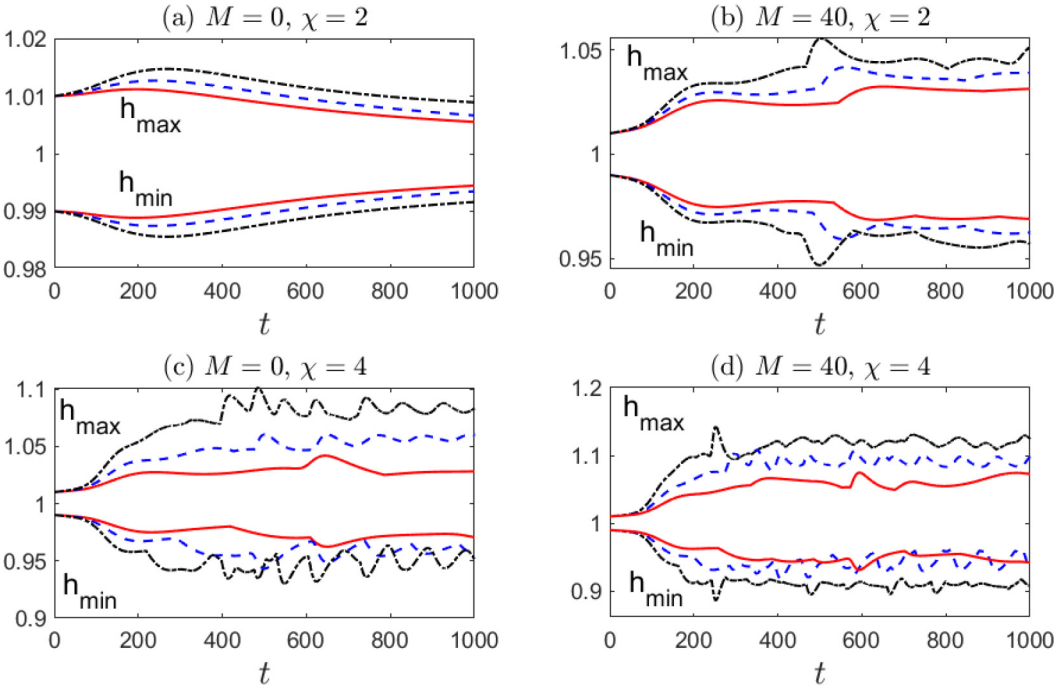

FIG. 21. Maximum ($h_{\max}$) and minimum ($h_{\min}$) amplitude of the film thickness [with initial profile equation (83)] for different viscoelastic parameters γ with $\beta = 0.1$, Ka $= 3000$, $\mathcal{B} = 10$, and $\varphi = \pi/4$. Here the solid lines (_____) is for $\gamma = 0$, dashed lines (_ _ _) indicate $\gamma = 0.1$, and dot-dashed lines ($- \cdot -$) represent $\gamma = 0.2$.

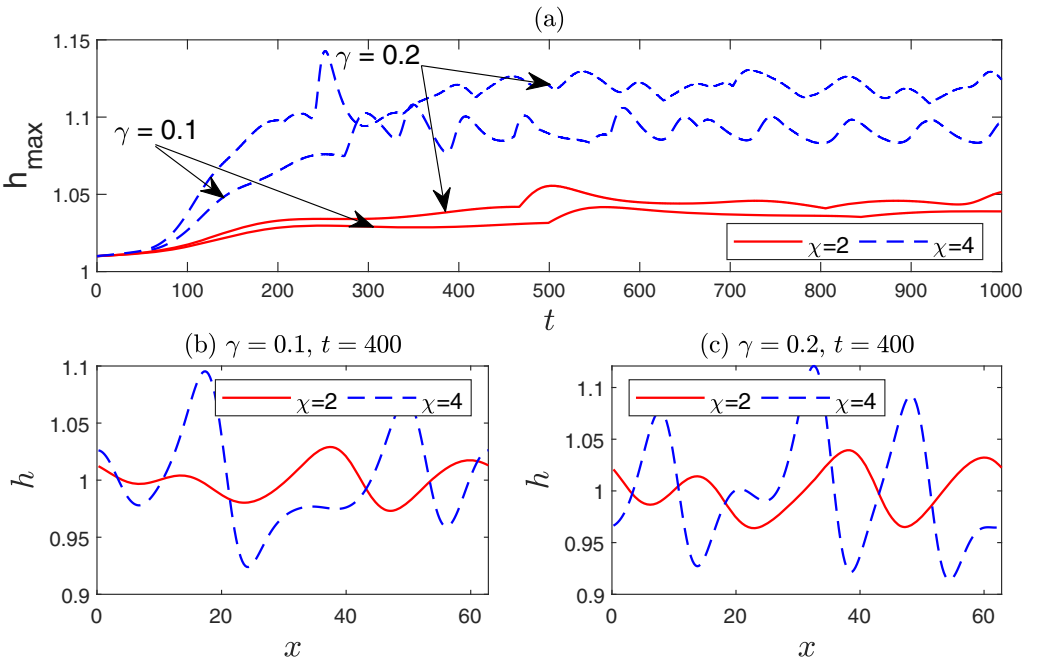

FIG. 22. Maximum amplitude and free-surface profiles of the film thickness [with initial profile equation (83)] for different viscoelastic parameter γ when $\beta = 0.1$, $M = 40$, Ka $= 3000$, $\mathcal{B} = 10$, and $\varphi = \pi/4$.

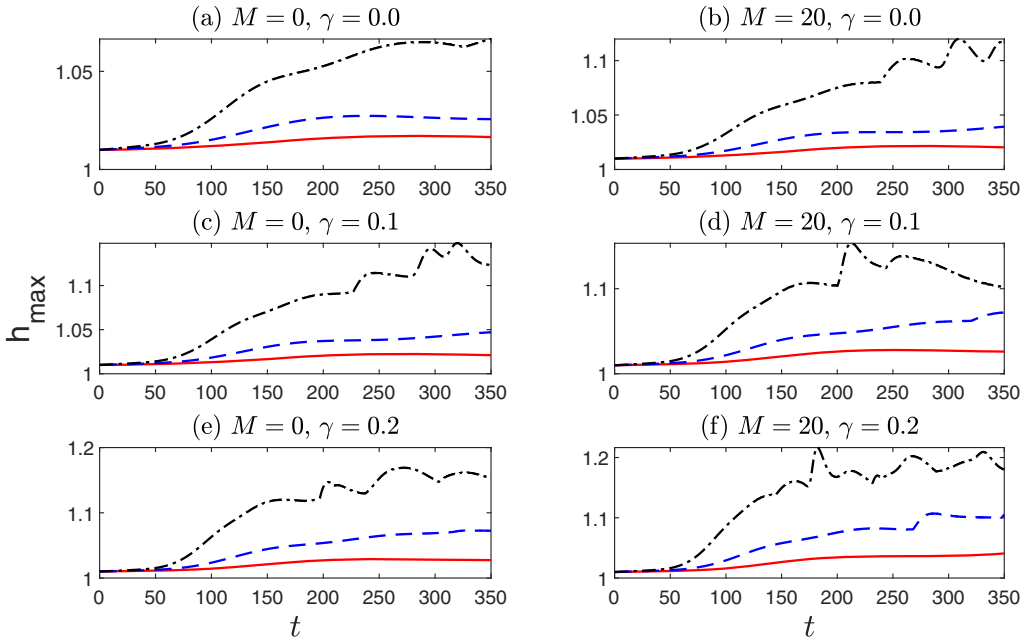

FIG. 23. Maximum amplitude of the film thickness h [with initial profile equation (83)] for different slip lengths β with $\chi = 4$, Ka $= 3000$, $\mathcal{B} = 10$, and $\varphi = \pi/4$. Here the solid lines (_____) is for $\beta = 0$, dashed lines (_ _ _) indicate $\beta = 0.1$, and dot-dashed lines ($- \cdot -$) represent $\beta = 0.2$.

VII. SUMMARY AND CONCLUSIONS

In this paper, we present the linear and nonlinear stability of a thin viscoelastic film flow along a uniformly heated slippery inclined plane. The model captures the thermocapillary effect and implements a Navier slip condition at the solid-liquid interface. We linearize the Navier-Stokes and the energy equations to obtain an eigenvalue problem involving the Orr-Sommerfeld-type equations. We obtain an expression for the critical Reynolds number for the instability of very long perturbations. Furthermore, we construct a nonlinear evolution equation in terms of the film thickness incorporating the effect of the slip length, viscoelasticity, and thermocapillarity. We introduce the Marangoni number M, slip length β, and viscoelastic parameter γ to characterize the thermocapillarity, slip length, and viscoelastic effect respectively. Results of linear stability analysis show that the instability of the flow is promoted by the slip length and the viscoelastic parameter. When the substrate is heated, the instability is reinforced. Using the method of multiple scales, weakly nonlinear stability analysis is performed. Based on this analysis, we have identified the existence of both subcritical unstable and supercritical stable regions. Finally, we numerically simulate the full thin-film model to demonstrate the role of the slip length, thermocapillarity, and viscoelastic parameter. Here we would like to mention one point that we have not considered the effect of fluid evaporation or condensation. Hence the present analysis is valid when the fluid is nonvolatile as well as when the evaporation or condensation of the liquid films is not taken into account. Future work will focus on experimental verification of the results presented in this paper as well as on exploring the dynamics of thin-film flows down the heated substrate in the scope of flows at moderate Reynolds numbers.

The data that support the findings of this study are available from the corresponding author upon reasonable request.

ACKNOWLEDGMENTS

We thank the two anonymous referees and the associate editor for their insightful comments and constructive suggestions on improving the paper.

S.C. conceptualized the work and A.S.D. conducted the MATLAB plots.

APPENDIX: EXPRESSIONS OF L_0, L_1, L_2, N_2, AND N_3

$$L_0 \equiv \frac{\partial}{\partial t} + A\frac{\partial}{\partial x} + B\frac{\partial^2}{\partial x^2} + C\frac{\partial^4}{\partial x^4}, \quad L_1 \equiv \frac{\partial}{\partial t_1} + A\frac{\partial}{\partial x_1} + 2B\frac{\partial^2}{\partial x \partial x_1} + 4C\frac{\partial^4}{\partial x^3 \partial x_1},$$

$$L_2 \equiv \frac{\partial}{\partial t_2} + B\frac{\partial^2}{\partial x_1^2} + 6C\frac{\partial^4}{\partial x^2 \partial x_1^2},$$

$$N_2 \equiv A'\eta_1\frac{\partial \eta_1}{\partial x} + B'\left[\eta_1\frac{\partial^2 \eta_1}{\partial x^2} + \left(\frac{\partial \eta_1}{\partial x}\right)^2\right] + C'\left[\eta_1\frac{\partial^4 \eta_1}{\partial x^4} + \frac{\partial \eta_1}{\partial x}\frac{\partial^3 \eta_1}{\partial x^3}\right],$$

$$\begin{aligned} N_3 \equiv{}& A'\left[\eta_1\left(\frac{\partial \eta_2}{\partial x} + \frac{\partial \eta_1}{\partial x_1}\right) + \eta_2\frac{\partial \eta_1}{\partial x}\right] + B'\left[\eta_1\left(\frac{\partial^2 \eta_2}{\partial x^2} + 2\frac{\partial^2 \eta_1}{\partial x \partial x_1}\right) + \eta_2\frac{\partial^2 \eta_1}{\partial x^2}\right. \\ &\left. + 2\frac{\partial \eta_1}{\partial x}\left(\frac{\partial \eta_2}{\partial x} + \frac{\partial \eta_1}{\partial x_1}\right)\right] + C'\left[\eta_1\left(\frac{\partial^4 \eta_2}{\partial x^4} + 4\frac{\partial^4 \eta_1}{\partial x^3 \partial x_1}\right) + \eta_2\frac{\partial^4 \eta_1}{\partial x^4} + \frac{\partial \eta_1}{\partial x}\left(\frac{\partial^3 \eta_2}{\partial x^3} + 3\frac{\partial^3 \eta_1}{\partial x^2 \partial x_1}\right)\right. \\ &\left. + \frac{\partial^3 \eta_1}{\partial x^3}\left(\frac{\partial \eta_2}{\partial x} + \frac{\partial \eta_1}{\partial x_1}\right)\right] + \frac{1}{2}A''\eta_1^2\frac{\partial \eta_1}{\partial x} + B''\left(\frac{1}{2}\eta_1^2\frac{\partial^2 \eta_1}{\partial x^2} + \eta_1\left(\frac{\partial \eta_1}{\partial x}\right)^2\right) \\ &+ C''\left(\frac{1}{2}\eta_1^2\frac{\partial^4 \eta_1}{\partial x^4} + \eta_1\frac{\partial \eta_1}{\partial x}\frac{\partial^3 \eta_1}{\partial x^3}\right). \end{aligned}$$

[1] A. Oron, S. H. Davis, and S. G. Bankoff, Long-scale evolution of thin liquid films, Rev. Mod. Phys. **69**, 931 (1997).

[2] R. Craster and O. K. Matar, Dynamics and stability of thin liquid films, Rev. Mod. Phys. **81**, 1131 (2009).

[3] S. Kalliadasis, C. Ruyer-Quil, B. Scheid, and M. G. Velarde, *Falling Liquid Films*, Applied Mathematical Sciences (Springer, 2012), p. 176.

[4] S. Chattopadhyay, A. Mukhopadhyay, and A. Barua, A review on hydrodynamical stability of thin film flowing along an inclined plane, J. Math. Sci. Model. **2**, 133 (2019).

[5] J. R. A. Pearson, On convection cells induced by surface tension, J. Fluid Mech. **4**, 489 (1958).

[6] C. V. Sternling and L. E. Scriven, Interfacial turbulence: Hydrodynamic instability and the Marangoni effect, AIChE J. **5**, 514 (1959).

[7] D. A. Goussis and R. E. Kelly, Surface wave and thermocapillary instabilities in a liquid film flow, J. Fluid Mech. **223**, 25 (1991).

[8] S. Kalliadasis, E. A. Demekhin, C. Ruyer-Quil, and M. G. Velarde, Thermocapillary instability and wave formation on a film falling down a uniformly heated plane, J. Fluid Mech. **492**, 303 (2003).

[9] S. George Bankoff, Stability of liquid flow down a heated inclined plane, Int. J. Heat Mass Transfer **14**, 377 (1971).

[10] S. W. Joo, S. H. Davis, and S. G. Bankoff, Long-wave instabilities of heated falling films: Two-dimensional theory of uniform layers, J. Fluid Mech. **230**, 117 (1991).

[11] P. G. Lopez, S. G. Bankoff, and M. J. Miksis, Non-isothermal spreading of a thin liquid film on an inclined plane, J. Fluid Mech. **324**, 261 (1996).
[12] P. M. J. Trevelyan and S. Kalliadasis, Wave dynamics on a thin-liquid film falling down a heated wall, J. Eng. Math. **50**, 177 (2004).
[13] C. Ruyer-quil, B. Scheid, S. Kalliadasis, M. G. Velarde, and R. Kh. Zeytounian, Thermocapillary long waves in a liquid film flow. Part 1. Low-dimensional formulation, J. Fluid Mech. **538**, 199 (2005).
[14] B. Scheid, C. Ruyer-Quil, S. Kalliadasis, M. G. Velarde, and R. Kh. Zeytounian, Thermocapillary long waves in a liquid film flow. Part 2. Linear stability and nonlinear waves, J. Fluid Mech. **538**, 223 (2005).
[15] P. M. J. Trevelyan, B. Scheid, C. Ruyer-Quil, and S. Kalliadasis, Heated falling films, J. Fluid Mech. **592**, 295 (2007).
[16] R. B. Bird, R. C. Armstrong, and O. Hassager, *Dynamics of Polymeric Liquids* (Wiley, 1987).
[17] D. W. Beard and K. Walters, Elastico-viscous boundary layer flows I. Two-dimensional flow near a stagnation point, Math. Proc. Cambridge Philos. Soc. **60**, 667 (1964).
[18] B. S. Dandapat and A. S. Gupta, Long waves on a layer of viscoelastic fluid down an inclined plane, Rheol. Acta **17**, 492 (1978).
[19] E. S. G. Shaqfeh, R. G. Larson, and G. H. Fredrickson, The stability of gravity driven viscoelastic film flow at low to moderate Reynolds number, J. Non-Newtonian Fluid Mech. **31**, 87 (1989).
[20] P. J. Cheng, H. Y. Lai, and C. K. Chen, Stability analysis of thin viscoelastic liquid film flowing down on a vertical wall, J. Phys. D: Appl. Phys. **33**, 1674 (2000).
[21] H. I. Andersson and E. N. Dahi, Gravity-driven flow of a viscoelastic liquid film along a vertical wall, J. Phys. D: Appl. Phys. **32**, 1557 (1999).
[22] B. Uma and R. Usha, Dynamics of a thin viscoelastic film on an inclined plane, Int. J. Eng. Sci. (Oxford, U. K.) **44**, 1449 (2006).
[23] B. S. Dandapat and A. Samanta, Bifurcation analysis of first and second order Benney equations for viscoelastic fluid flowing down a vertical plane, J. Phys. D: Appl. Phys. **41**, 095501 (2008).
[24] N. Amatousse, H. Ait Abderrahmane, and N. Mehidi, Traveling waves on a falling weakly viscoelastic fluid film, Int. J. Eng. Sci. (Oxford, U. K.) **54**, 27 (2012).
[25] Q. Fu, T. Hu, and L. Yang, Instability of a weakly viscoelastic film flowing down a heated inclined plane, Phys. Fluids **30**, 084102 (2018).
[26] A. Sharma, P. K. Ray, and D. T. Papageorgiou, Dynamics of gravity-driven viscoelastic films on wavy walls, Phys. Rev. Fluids **4**, 063305 (2019).
[27] M. H. Allouche, V. Botton, S. Millet, D. Henry, S. D. Bohy, B. Güzel, and H. B. Hadid, Primary instability of a shear-thinning film flow down an incline: Experimental study, J. Fluid Mech. **821**, R1 (2017).
[28] J. P. Pascal, Linear stability of fluid flow down a porous inclined plane, J. Phys. D: Appl. Phys. **32**, 417 (1999).
[29] G. S. Beavers and D. D. Joseph, Boundary conditions at a naturally permeable wall, J. Fluid Mech. **30**, 197 (1967).
[30] A. Samanta, C. Ruyer-Quil, and G. Benoit, Falling film down a slippery inclined plane, J. Fluid Mech. **684**, 353 (2011).
[31] R. Voronov, D. Papavassiliou, and L. Lee, Review of fluid slip over superhydrophobic surfaces and its dependence on the contact angle, Ind. Eng. Chem. Res. **47**, 2455 (2008).
[32] S. Chakraborty, T. W. Sheu, and S. Ghosh, Dynamics and stability of a power-law film flowing down a slippery slope, Phys. Fluids **31**, 013102 (2019).
[33] A. Samanta, Non-modal stability analysis in viscous fluid flows with slippery walls, Phys. Fluids **32**, 064105 (2020).
[34] S. Chattopadhyay, Influence of the odd viscosity on a falling film down a slippery inclined plane, Phys. Fluids **33**, 062106 (2021).
[35] Z. Ding and T. N. Wong, Falling liquid films on a slippery substrate with Marangoni effects, Int. J. Heat Mass Transfer **90**, 689 (2015).
[36] E. Ellaban, J. P. Pascal, and S. J. D. D'Alessio, Instability of a binary liquid film flowing down a slippery heated plate, Phys. Fluids **29**, 092105 (2017).

[37] S. Chattopadhyay, A. Mukhopadhyay, A. K. Barua, and A. K. Gaonkar, Thermocapillary instability on a film falling down a non-uniformly heated slippery incline, Int. J. Non-Linear Mech. **133**, 103718 (2021).
[38] S. Chattopadhyay, A. S. Desai, A. K. Gaonkar, A. K. Barua, and A. Mukhopadhyay, Weakly viscoelastic film on a slippery slope, Phys. Fluids **33**, 112107 (2021).
[39] J. G. Savins, A stress-controlled drag-reduction phenomenon, Rheol. Acta **6**, 323 (1967).
[40] S. Pal and A. Samanta, Linear stability of a surfactant-laden viscoelastic liquid flowing down a slippery inclined plane, Phys. Fluids **33**, 054101 (2021).
[41] I. M. R. Sadiq and R. Usha, Linear instability in a thin viscoelastic liquid film on an inclined, non-uniformly heated wall, Int. J. Eng. Sci. (Oxford, U. K.) **43**, 1435 (2005).
[42] R. Sarma and P. K. Mondal, Marangoni instability in a heated viscoelastic liquid film: Long-wave versus short-wave perturbations, Phys. Rev. E **100**, 013103 (2019).
[43] K. Walters, The motion of an elastico-viscous liquid contained between co-axial cylinders (II), Q. J. Mech. Appl. Math. **13**, 444 (1960).
[44] A. Samanta, Role of slip on the linear stability of a liquid flow through a porous channel, Phys. Fluids **29**, 094103 (2017).
[45] A. Mukhopadhyay and S. Chattopadhyay, Long wave instability of thin film flowing down an inclined plane with linear variation of thermophysical properties for very small Biot number, Int. J. Non-Linear Mech. **100**, 20 (2018).
[46] S. Chattopadhyay, Odd-viscosity-induced instability of a thin film with variable density, Phys. Fluids **33**, 082102 (2021).
[47] I. M. R. Sadiq, R. Usha, and S. W. Joo, Instabilities in a liquid film flow over an inclined heated porous substrate, Chem. Eng. Sci. **65**, 4443 (2010).
[48] I. S. Khattab, F. Bandarkar, M. A. A. Fakhree, and A. Jouyban, Density, viscosity, and surface tension of water+ethanol mixtures from 293 to 323 K, Korean J. Chem. Eng. **29**, 812 (2012).
[49] T. B. Benjamin, Wave formation in laminar flow down an inclined plane, J. Fluid Mech. **2**, 554 (1957).
[50] C. S. Yih, Stability of liquid flow down an inclined plane, Phys. Fluids **6**, 321 (1963).
[51] Anjalaiah and R. Usha, Effects of velocity slip on the inertialess instability of a contaminated two-layer film flow, Acta Mech. **226**, 3111 (2015).
[52] D. A. Nield and A. Bejan, *Convection in Porous Media* (Springer, 2006).
[53] R. Usha and B. Uma, Long waves on a viscoelastic film flow down a wavy incline, Int. J. Non-Linear Mech. **39**, 1589 (2004).
[54] B. Uma and R. Usha, Interfacial phase change effects on the stability characteristics of thin viscoelastic liquid film down a vertical wall, Int. J. Eng. Sci. (Oxford, U. K.) **42**, 1381 (2004).
[55] U. Thiele, B. Goyeau, and M. G. Velarde, Stability analysis of thin film flow along a heated porous wall, Phys. Fluids **21**, 014103 (2009).
[56] A. Oron and O. Gottlieb, Subcritical and supercritical bifurcations of the first- and second-order benney equations, J. Eng. Math. **50**, 121 (2004).
[57] I. M. R. Sadiq and R. Usha, Thin newtonian film flow down a porous inclined plane: Stability analysis, Phys. Fluids **20**, 022105 (2008).
[58] A. Mukhopadhyay, S. Chattopadhyay, and A. K. Barua, Effects of strong viscosity with variable fluid properties on falling film instability, in *Advances in Nonlinear Dynamics*, NODYCON Conference Proceedings Series, edited by W. Lacarbonara, B. Balachandran, M. J. Leamy, J. Ma, J. A. Tenreiro Machado, and G. Stepan (Springer, 2022), pp. 75–85.
[59] Y. Chao, Z. Ding, and R. Liu, Dynamics of thin liquid films flowing down the uniformly heated/cooled cylinder with wall slippage, Chem. Eng. Sci. **175**, 354 (2018).
[60] S. Chattopadhyay, G. Y. Subedar, A. K. Gaonkar, A. K. Barua, and A. Mukhopadhyay, Effect of odd-viscosity on the dynamics and stability of a thin liquid film flowing down on a vertical moving plate, Int. J. Non-Linear Mech. **140**, 103905 (2022).